ISSN: 2764-5886
e-ISSN: 2764-622X

Volume 5· Nº 3 · September 2022

Journal of Bioengineering, Technologies and Health

An Official Publication of
SENAI CIMATEC

ISSN: 2764-5886 / e-ISSN 2764-622X

Volume 5 • Number 3 • September 2022

JOURNAL OF BIOENGINEERING TECHNOLOGIES AND HEALTH

An Official Publication of SENAI CIMATEC

PUBLISHED BY SENAI CIMATEC

Sistema FIEB | SENAI CIMATEC
PELO FUTURO DA INOVAÇÃO

September 2022
Printed in Brazil

JOURNAL OF BIOENGINEERING, TECHNOLOGIES AND HEALTH

An Official Publication of SENAI CIMATEC

JOURNAL OF BIOENGINEERING AND TECHNOLOGY APPLIED TO HEALTH

Volume 5 • Number 3 *September 2022*

SUMMARY

Original Articles

Review Articles

The Journal of Bioengineering, Technologies and Health (JBTH) is an official publication of the SENAI CIMATEC (Serviço Nacional de Aprendizagem Industrial - Centro Integrado de Manufatura e Tecnologia). It is published quarterly (March - June - September - December) in English by SENAI CIMATEC – Avenida Orlando Gomes, 1845, Piatã, Zip Code: 41650-010, Salvador-Bahia-Brazil; phone: (55 71) 3879-5501. The editorial offices are at SENAI CIMATEC.

Editorial Office

Correspondence concerning subscriptions, advertisements, claims for missing issues, changes of address, and communications to the editors should be addressed to the Deputy Editor, Dr. Roberto Badaró, SENAI CIMATEC (Journal of Bioengineering, Technologies and Health – JBTH) – Avenida Orlando Gomes, 1845, Piatã, Zip code: 41650-010, Salvador-Bahia-Brazil; phone: (55 71) 3879-5501; or sent by e-mail: jbth@fieb.org.br / jbth.cimatec@gmail.com.

Permissions

The permissions should be asked to the Ediot in Chief of the Journal of Bioengineering, Technologies and Health and SENAI CIMATEC. All rights reserved. Except as authorized in the accompanying statement, no part of the JBTH may be reproduced in any form or by any electronic or mechanic means, including information storage and

COVER: The free high-resolution photo of light, sunlight, atmosphere, skyscraper, environment, line, green, reflection, environmental, electricity, solar, wind energy, energy, ecology, collage, renewable energy, bamboo, sustainable, generation, renewable, photovoltaic, renewables, taken with an unknown camera on April 2017. Creative Commons CC0.

Postmaster

Send address changes to JBTH, Avenida Orlando Gomes, 1845, Piatã, Zip Code: 41650-010, Salvador-Bahia-Brazil.

Information by JBTH-SENAI CIMATEC

Address: Avenida Orlando Gomes, 1845, Piatã, Zip Code: 41650-010, Salvador-Bahia-Brazil
Home-page: www.jbth.com.br
E-mail: jbth@fieb.org.br / jbth.cimatec@gmail.com
Phone: (55 71) 3879-5501 / 3879-5500 / 3879-9500

DOI:10.34178/jbth.v5i3

Characterization of Polyvinyl Butyral and Sentryglas® Polymers Used as Interlayers in Laminated Glass

Gislana Santana Machado[1*], Willams Teles Barbosa[1], Josiane Dantas Viana Barbosa[1]
[1]SENAI CIMATEC University Center; Salvador, Bahia Brazil

The polymers used as interlayers in the laminated glass support the tensile stresses, keeping the glass fragments fixed in the film and avoiding possible accidents. This article aims to characterize the polymers Polyvinyl Butyral and Sentryglas®, as their physical-chemical and mechanical properties. It may help a laminated glass company located in Bahia to optimize its production process. We tested the samples to Fourier Transform Infrared Spectroscopy (FTIR), Thermogravimetric Analysis (TGA), and Tensile. The results allowed us to characterize the materials technically, comparing them with the data from the sheets provided by their manufacturer. In addition, it has provided the Laminated Glass Factory with data that can reduce costs and improve production.
Keywords: Laminated Glass. Polymers. Polyvinyl Butyral. Sentryglas®.

Introduction

The glass lamination process consists of two or more layers of glass intercalated with one or more films, which increases its mechanical resistance. In addition, the intermediate layer supports the tensile stresses, preventing the glass fragments from detaching in case of breakage, making it a safety glass. The intercalary material can be PVB (Polyvinyl Butyral), SGA (Sentryglas®), and others [1,2].

PVB is a nonlinear viscoelastic material with deformability and sensitivity to temperature [2]. The reaction of polyvinyl alcohol with butyraldehyde produces PVB, characterized as a random amorphous termopolymer [3,4]. Due to its mechanical properties, PVB is widely used as a protective film, especially in the automotive industry, where vehicle windshields have laminated glass [5].

SGA film is an ionomer that has a structure composed of hydrocarbons with acid groups, commonly obtained by copolymerization of olefins (ethylene, butadiene, or styrene) and functionalized monomers (acrylic acid, p-styrene sulfonic acid, or methacrylic acid) [6]. The American company DuPont developed this film for the glass facades to resist hurricanes in the United States. Furthermore, due to its mechanical and durability advantages, the film's use expanded in areas where storms do not occur [1]. In Bahia (Brazil), a laminated glass factory provides glass solutions focused on processing monolithic and tempered glass by laminating them to make them resistant and safe glass. To improve the company's productivity, reduce costs, and optimize its process, we studied the properties of PVB and SGA, which are the interlayers used by the company.

The objective is to have better process control because the quality of the laminated glass depends directly on the behavior of the film when it adheres to the glass. In the lamination process, sequences of heating are carried out so that possible delamination does not occur, which is the separation of the glass after the product is ready or imperfections that could prevent the commercialization of the product. In addition, proper conditioning of the PVB, with temperature and humidity control, can have its physical-chemical properties compromised due to its ability to absorb water and thus lose resistance.

For this reason, this study aimed to evaluate the physicochemical and mechanical properties of PVB films with and without conditioning. For comparison, we also achieved the characterization of the SGA film. This work consists of exploratory, experimental research, quantitative and qualitative.

Received on 16 June 2022; revised 15 August 2022.
Address for correspondence: Gislana Santana Machado. Av. Orlando Gomes, 1845 - Piatã, Salvador - BA- Brazil. Zipcode: 41650-010. E-mail: gislana.machado@aln.senaicimatec.edu.
DOI 10.34178/jbth.v5i3.221.

J Bioeng. Tech. Health 2022;5(3):160-167.

Materials and Methods

Materials

We collected the PVB and SGA films in a lamination industry in Bahia, Brazil.

PVB

The Japanese company Kuraray Co., Ltd. produced the PVB films collected. Table 1 shows the properties of PVB film made available from Kuraray.

Table 1. PVB properties [7].

Properties	Values
Density (g/cm³)	1.065
Tensile strength (MPa)	> 23
Tensile elongation (%)	> 280

We collected six PVB films with dimensions of 280 x 200 x 1.52 mm. Three films were hermetically wrapped in aluminum foil (PVB A) and kept at a controlled temperature of 17 ± 5°C and humidity of 21 ± 7%. And we kept the other three films in an uncontrolled environment (PVB NA).

SGA

The Japanese company Kuraray Co., Ltd. also produced the SGA films collected. Table 2 presents the properties of the SGA film made available by Kuraray.

Table 2. SGA properties [8].

Properties	Values
Density (g/cm³)	0.95
Tensile strength (MPa)	34.5
Tensile elongation (%)	400

We collected three SGA films with dimensions of 280 x 200 x 0.76 mm. There was no need to keep the SGA films in an environment with controlled temperature and humidity since these parameters do not affect the physicochemical properties of the material [8,9].

Methods

We characterized the films by Fourier Transform Infrared Spectroscopy (FTIR) in a Nicolet iS 10 (Thermo Scientific, Massachusetts, USA) with a spectral range of 4000 to 400 cm^{-1}, resolution of 4 cm^{-1}, and 32 scans. TA Instruments DSC model Q3 analyzer (TA Instruments, New Castle, USA) performed the thermogravimetric (TGA) with a heating rate of 10 °C/min in a nitrogen atmosphere over a temperature range of 25 °C to 700 °C. The uniaxial tensile tests were performed in a universal machine model DL 2000 (EMIC, São Paulo, Brazil) under a constant displacement rate of 50 mm/min, according to ISO 527-1 [10]. For the tensile test, we cut the film in the "tie" model (type IVB), and the ASTM D638 standard determined the dimensions [11] (Figure 1). Ten specimens were used for each type of film to ensure repeatability and a well-defined curve.

Figure 1. Tensile specimen dimensions, based on ASTM D638 standard [11].

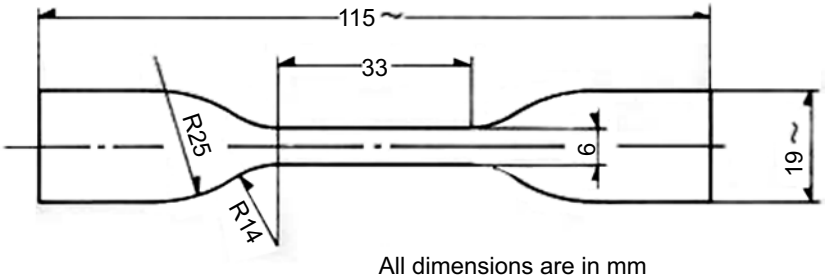

Results and Discussion

Fourier Transform Infrared Spectroscopy – FTIR

Figure 2 shows the FTIR spectra of PVB A and PVB NA films.

We observed that PVB A and PVB NA showed similar FTIR spectra, corroborating the results of Xiang and colleagues [12]. Table 3 describes the characteristics of each band identified in the FTIR spectra of PVB A and PVB NA.

We verified a slight shift of the band related to the OH group for the PVB NA film (3434.41 cm^{-1}) compared to the spectrum of PVB A (3402.54 cm^{-1}) (Table 3). This displacement may result from water absorption, thus changing the molecular structure of the PVB NA film. We considered that PVB is an amorphous random terpolymer having as a composition the monomers vinyl butyral (76%-80% by weight), which is a substance that does not absorb water and has elastic properties. And vinyl alcohol (18%-22% by weight) and vinyl acetate (1%-2% by weight), substances that can absorb water. In addition to providing better adhesion to inorganic materials such as glass [6,13]. Figure 3 shows the FTIR spectrum for the SGA film.

The spectrum observed for the SGA film (Figure 3) shows characteristic bands of polyethylene and methacrylic acid [14]. Table 4 describes the characteristics of each band identified in the FTIR spectra of SGA.

The FTIR results (Table 4) confirm that there was no change in the chemical properties of the SGA film. With bands characteristic of an ionomer based on poly (ethylene methacrylic acid) [9].

Thermogravimetric Analysis – TGA

Figure 4 shows the TG and DTG curves of the PVB A film.

Figure 4 shows three mass loss events identified in the DTG curve. Events 1-3 occur at 215.92°C, 294.65°C, and 388.03°C, respectively. Figure 5 shows the TG and DTG curves of the PVB NA film.

Analyzing the thermal behavior of the PVB NA film (Figure 5), we identify three mass loss events at the DTG curve. The first occurs at 218.01°C, the second at 288.18°C, and the third at 382.17°C. We observed similar thermal behavior when comparing the TGA results of PVB A (Figure 4) and PVB NA' (Figure 5) films. The mass reduction in the first two events for the P films is related to the OH (Hydroxyl) group, with

Figure 2. FTIR spectra of PVB A and PVB NA films.

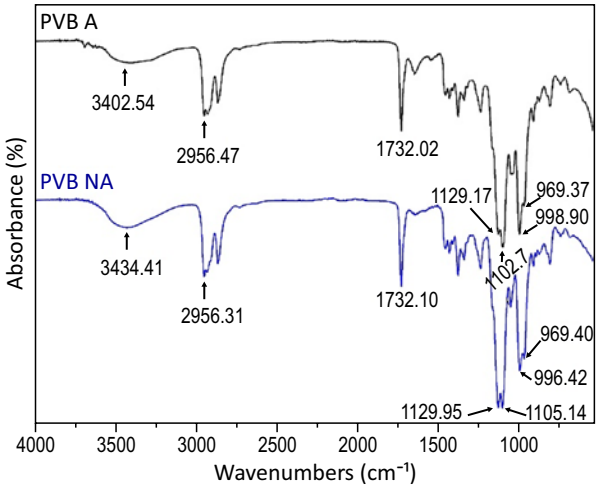

Table 3. Description of the FTIR results of PVB A and PVB NA.

Wavenumber (cm^{-1}) PVB A	PVB NA	Characteristics	Similar Band Material
3402.54	3434.41	Stretching vibration of OH (Hydroxyl)	Vinyl alcohol
2956.47	2956.31	C-H (Hydrocarbon) stretching vibration	-
1732.02	1732.1	Elongation vibration of C=O (Carbonyl)	Acetate vinyl
1129.17	1129.95	Shear bending vibration of the CH_2 (Hydrocarbon) group	Vinyl butyral
1102.77	1105.14	Shear bending vibration of the CH_3 (Methyl) group	Vinyl butyral
998.90	996.42	C-O-C stretching vibration (Ether)	-
969.37	969.4	C-O stretching vibration (Carbon Monoxide)	-

Figure 3. FTIR spectrum of the SGA film.

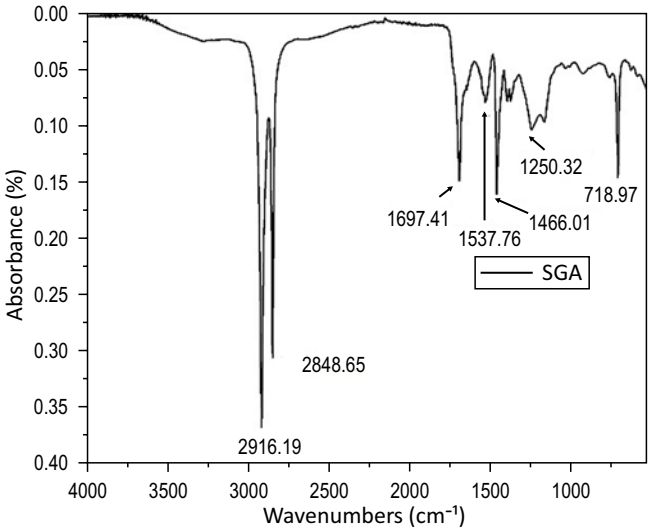

water loss. In the third event, the degradation of the butyric group $(C_8H_{14}O_2)n$ occurs [12]. In the second event, there was a more significant mass loss for the PVB NA film (30.26%), higher than PVB A, with a loss of 28.72%. This higher mass loss of the PVB NA can be justified by water absorption because an environment with controlled humidity cannot store this material.

Figure 6 shows the TG and DTG curves of the SGA film, and we can analyze two mass loss events. The first is at 425.78°C, and the second is at 472.80°C. Because it is a structural film, there was a considerable mass loss of 90.96% above 400°C. According to Yifan and colleagues [15], this mass loss is related to the volatilization of the decomposed polymer chain. Comparing the TG/DTG curves of

Table 4. Description of the FTIR Results of the SGA.

Wavenumber (cm^{-1})	Characteristics	Similar Band Material
2916.19	Asymmetric CH_2 stretching absorption (Hydrocarbon)	Polyethylene and methacrylic acid
2848.65	CH_2 symmetric stretching absorption (Hydrocarbon)	Polyethylene and methacrylic acid
1697.41	Symmetric stretching absorption of C=O (Carbonyl) of carboxylic acid	Methacrylic Acid
1537.76	Asymmetric stretching absorption of RCOO- (carboxylate group)	Methacrylic Acid
1466.01	Superposition of absorption with asymmetric bending vibration of the CH_3 (Methyl) group and shear bending of CH_2 (Hydrocarbon)	Polyethylene and methacrylic acid
1250.32	O-C(=O)-C (ester) stretching absorption	Methacrylic Acid
718.97	Balance-type bending absorption of CH_2 (Hydrocarbon) groups when linked in a sequence of 4 or more.	Polyethylene and methacrylic acid

Figure 4. TG and DTG curves of PVB A film.

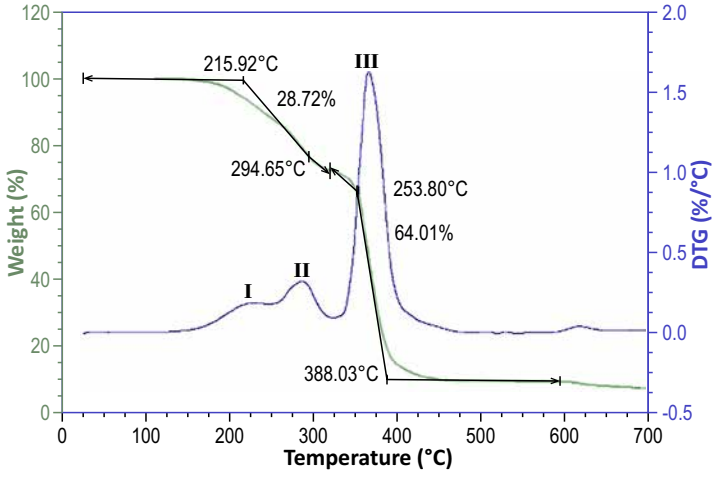

the PVB films and SGA, we can verify that the SGA has a higher thermal resistance, presenting no mass loss in the temperature range of 25°C to 400°C. On the other hand, in this same range, the PVB goes through 3 mass loss events due to the -COONa (carboxylic acid) group providing additional ionic strength to SGA compared to PVB [15,16].

Tensile Tests

Figure 7 shows the stress-strain curves for PVB A, PVB NA, and SGA films.

The stress-strain curves of PVB films have a small nonlinear elastic area, and a region in which their stiffness gradually increases until rupture

Figure 5. TG and DTG curves of PVB NA film.

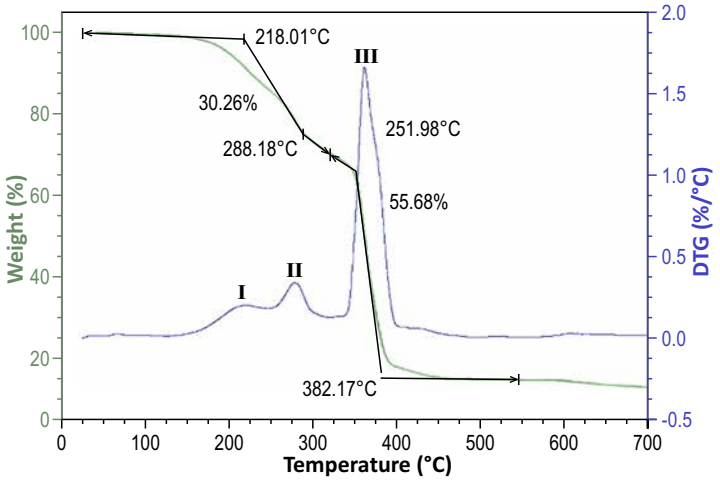

Figure 6. TG and DTG curves of SGA film.

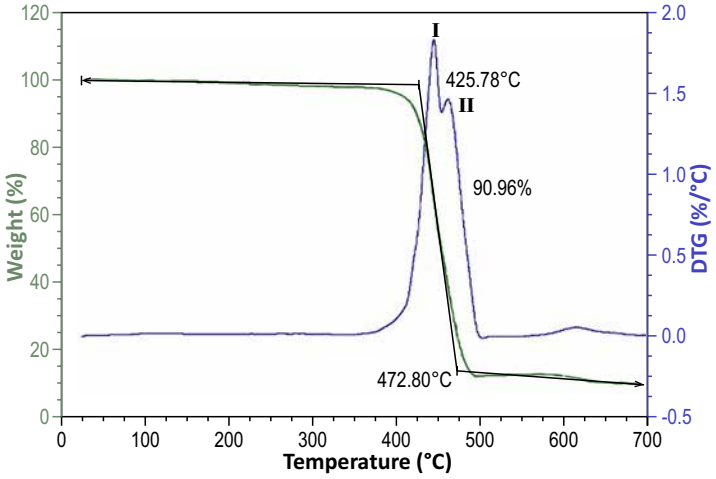

Figure 7. Stress-strain curves of PVB A, PVB NA, and SGA films.

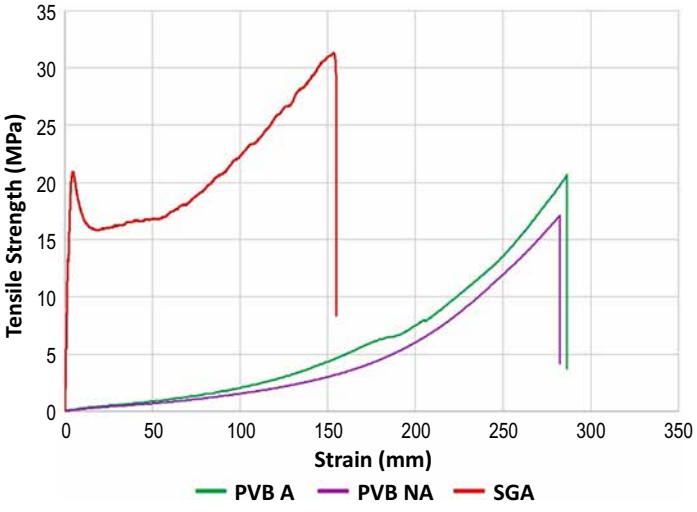

[Figure 8 (b)], characteristic behavior of an elastomer [17,18]. Therefore, PVB is considered a hyperelastic material, in which the stretching of the mesh becomes increasingly tricky as the chains are tractioned, resulting in its stiffening [19]. Besides this, because it is a hygroscopic polymer, it quickly absorbs water, which can interfere with its mechanical properties [6]. The stress-strain curve of the SGA presents a small initial nonlinear region, followed by an elastic zone. Subsequently, a second region with lower stiffness than the initial one characterizes a plastic behavior. Finally, an increase in stiffness until the strain of the specimen (Figure 8 (d)) implies a behavior characteristic of a plastic material [17].

Table 5 shows the uniaxial tensile test data for PVB A, PVB NA, and SGA films.

About the tensile test of films (Table 5), we observed that the PVB A showed maximum stress of 20.69 MPa, higher than the PVB NA with a pressure of 17.08 MPa. This loss of resistance of the PVB NA film is mainly related to water absorption, occurring in the degradation of the material. The tensile strength of SGA (31.35 MPa) is higher than PVB A and PVB NA, 20.69 and 17.08 MPa, respectively. Because it is a hydrophobic ionomer, it does not absorb water. This polymer is composed of ionic groups, which increases the intermolecular forces between the polymer chains, forming a cross-linked structure and providing greater mechanical tensile strength [8,15,20]. PVB A and PVB NA films had results lower than those stipulated by the manufacturer, which is 23 MPa (Table 1) [7]. The SGA also showed lower tensile strength (31.35 MPa) than that specified by the manufacturer, which is 34.5 MPa (Table 2) [8]. The tensile strength values of the films can vary according to the method applied and the equipment used for the tests.

Figure 8. PVB specimens before (a) and after (b) tensile test. And SGA specimens before (c) and after (b) tensile test.

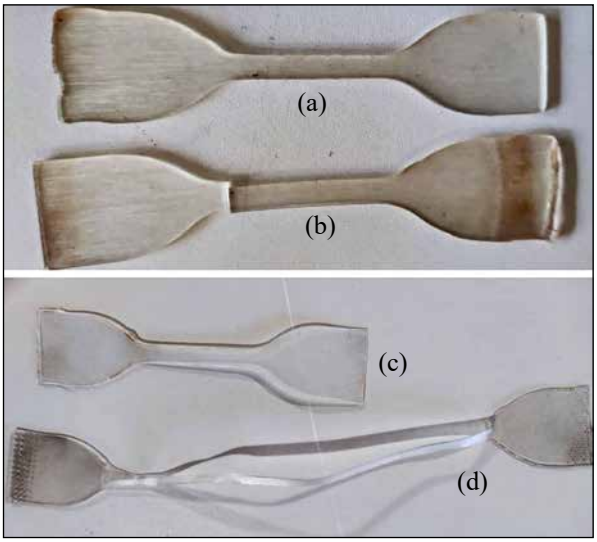

Table 5. Tensile test data of PVB A, PVB NA, and SGA films.

Properties	PVB A	PVB NA	SGA
Tensile Strength (MPa)	20.69	17.08	31.35
Deformation (%)	286.89	276.14	158.32

Conclusions

The FTIR analysis revealed a change in the molecular structure of the PVB films due to the water absorption of the PVB NA film. The SGA showed characteristic bands of the material. PVB A and PVB NA films showed similar thermal behavior, but there was a more significant initial mass loss for PVB NA due to water absorption from the environment. The tensile stress tests showed a decrease in strength for PVB NA compared to PVB A, confirming that water absorption caused the material to lose power. As expected, SGA showed higher tensile stress than PVB films because it is an ionomer. According to the results obtained in this study, it will be possible to establish storage parameters and optimize the production process to reduce production costs.

Acknowledgment

The authors thank SENAI CIMATEC for supporting the research.

References

1. Yujia L, Suwen C, Xiao S. Shear modulus of ionomer interlayer: Effects of time, temperature and strain rate. Construction and Building Materials 2021;302:124-224.
2. Xing C, Suwen C, Guo-Qiang L. Experimental investigation on the blast resistance of framed PVB-laminated glass. International Journal of Impact Engineering 2021;149(103):788.
3. Syaoira S, et al. Tensile strength and moisture absorption of sugar palm-polyvinyl butyral laminated composites. Polymers 2020;12(9):1923.
4. Motlatle AM, et al. The thermal degradation kinetics and morphology of poly (vinyl butyral) cast films prepared using different organic solvents. In: AIP Conference Proceedings. AIP Publishing LLC, 2020. p. 020071.
5. Shariari M, Googarchin HS. Prediction of vehicle impact speed based on the post-cracking behavior of automotive PVB laminated glass: Analytical modeling and numerical cohesive zone modeling. Engineering Fracture Mechanics 2020;240:107352.
6. Martin M, et al. Polymeric interlayer materials for laminated glass: A review. Construction and building materials 2020;230:116897.
7. Kuraray. Kuraray Trosifol™ – Trosifol® Architectural Laminated Glass Interlayers, 2017. Disponível em:< https://stargrup.com.tr/wp-content/uploads/2019/02/Trosifol-PVB-Data-Sheet.pdf> Acesso em 26, ago. 2022.
8. Kuraray. Kuraray Trosifol™ – Trosifol® Sentryglas®, 2019. Disponível em:< https://www.trosifol.com/fileadmin/user_upload/TROSIFOL/support/downloads/product_brochures/pdf_documents/sentryglas/SentryGlas_8_2019_engl_web.pdf>. Acesso em 26, ago. 2022.
9. Oliveira FR. Efeito da Incorporação de Aparas do Ionômero Sentryglas nas Propriedades de Engenharia do PEAD e do PEBD. Centro Universitário FEI, São Bernardo do Campo, 2018.
10. International Standard. ISO 527-1: Plastics - Determination of tensile properties - Part 1: General principles. 2012.
11. ASTM International. D638 – 14. Standard test method for tensile properties of plastics. ASTM International, 2014.
12. Xiang H, Yaxue L, Guiyin F. Thermal properties of polyvinyl butyral/graphene composites as encapsulation materials for solar cells. Solar Energy 2018;161:187-193.
13. Silva MLPG. Definição de práticas operacionais padrão em polímeros para fins de importação. Universidade Federal de Itajubá, 2017.
14. Oliveira FR. Efeito da Incorporação de Aparas do Ionômero Sentryglas nas Propriedades de Engenharia do ABS. 2016. 83 f. TFC (Graduação em Engenharia de Materiais) – Centro Universitário FEI, São Bernardo do Campo, 2016.
15. Yifan S, et al. Surlyn resin ionic interlayer-based laminated glass: preparation and property analysis. Advanced Composites and Hybrid Materials 2022;5(1):229-237.
16. Kozlowski M, et al. Structural considerations on timber-glass composites at fire scenarios. In: Challenging Glass Conference Proceedings 2018:229-240.
17. Centelles X, et al. Tensile test on interlayer materials for laminated glass under diverse ageing conditions and strain rates. Construction and Building Materials 2020;243:118230.
18. Valio GT. Estudo termodinâmico, microrreológico e de propriedades mecânicas de blendas poliméricas ternárias com matriz de PCL. 2020.Tese de Doutorado. Universidade de São Paulo, 2020.
19. Elzière P, et al. Supramolecular structure for large strain dissipation and outstanding impact resistance in polyvinylbutyral. Macromolecules 2019;52(20):7821-7830.
20. Hána T, et al. Experimental investigation of temperature and loading rate effects on the initial shear stiffness of polymeric interlayers. Engineering Structures 2020;223:110728.

Computational Model for Photovoltaic Solar Energy Forecasting Based on the K-Nearest Neighbor Method

Oberdan Pinheiro Rocha[1]*, Alexandre Menezes da Silva[1], Alex Álisson Bandeira Santos[1]
[1]SENAI CIMATEC University Center; Salvador, Bahia Brazil

Integrating PV technologies into power systems requires precise planning of PV performance. The ability to predict solar photovoltaic generation is a challenge for its integration into electrical systems. Improvements in forecasting models with more accurate results and fewer errors are necessary for the future development of microgrid projects and the dispatch of the economic sector. This research presents a computational machine learning model to predict the PV output power using historical PV output power data from a 960 kWP grid-connected PV system in southern Italy. The results showed agreement between the predicted and actual values, with errors ranging from 5% to 12%. We concluded that using machine learning techniques makes it feasible to predict the photovoltaic output power.
Keywords: Photovoltaic Power Forecast. Machine Learning. Regression.

Introduction

Solar energy is a friendly environment renewable energy source, making it a potential source of energy for industrial development [1]. Between 2017 and 2018, global photovoltaic power generation increased from 405 GW to 505 GW, representing 2.4% of total renewable energy [2]. In recent years, solar energy has experienced rapid growth in both developing and developed countries. There are several solar applications, such as photovoltaics, solar thermal, and other solar projects; however, solar radiation data is critical in each of them [3]. Although photovoltaic technology is a technological advancement, there is still a need for more research and development to improve the system's varied components.

Due to the complex nature of the operating conditions of photovoltaic systems, comprehending these elements is a significant challenge. In this sense, improving the techniques for measuring the power produced by photovoltaic generators is a strategy that can help the energy generation sector. According to IEA [4], there is an exponential increase in new renewable energies, such as wind and photovoltaic solar energy, in a Brazilian electrical matrix, presenting relevant technological evolution. The generation of photovoltaic solar energy depends fundamentally on solar irradiation at ground level, incident on a horizontal plane that is influenced by meteorological factors (cloud cover, rainfall, ambient temperature, atmospheric pressure, wind direction, humidity). These characteristics have promoted a broad spectrum of studies and the development of methods, techniques, and forecasting models.

This research aims to present a Computational Model for Photovoltaic Solar Energy Forecasting based on the k-nearest neighbor method. We organized two basic modules to propose the computational model: (i) data processing; and (ii) prediction model.

Studies

There are many studies on predicting the power generated by a photovoltaic module in the literature. Techniques involving machine learning, deterministic and hybrid techniques are examples [5]. Machine learning approaches investigated for power estimation of photovoltaic plants include multiple linear regression, support vector machine, adaptive neuro-fuzzy inference, and artificial neural networks. The research attempts to understand the relationship between outputs by adequately evaluating the data set, including acquired output and input parameters. Among them, ANN has been

Received on 26 June 2021; revised 22 August 2022.
Address for correspondence: Oberdan Pinheiro Rocha. Av. Orlando Gomes, 1845 - Piatã, Salvador - BA- Brazil. Zipcode: 41650-010. E-mail: oberdan.pinheiro@fieb.org.br. DOI 10.34178/jbth.v5i3.222.

J Bioeng. Tech. Health 2022;5(3):168-172.

widely applied [6]. Al-Amoudi and Zhang [7] developed a radial basis function neural network for peak power point prediction and solar panel modeling. The proposed method saves energy and accurately measures the maximum power without searching for the optimal power point.

Almonacid and colleagues applied an artificial neural network to estimate the photovoltaic output power. The results of this study showed that the artificial neural network technique produces significant improvements over traditional approaches. For example, artificial neural network errors range from 6% to 8%, while conventional approaches have errors ranging from 6% to 30% (taking into account only the effect of temperature and solar irradiance).

Mellit and Kalogirou used adaptive neuro-fuzzy inference to model and simulate photovoltaic plants. The proposed model predicts and simulates diverse electrical data from a photovoltaic energy system using solar irradiance, ambient temperature, and clarity index. Fonseca and colleagues [10] investigated the application of a support vector machine to predict the annual photovoltaic output power of a 1 MW photovoltaic plant. In addition, cloudiness was numerically predicted to examine how it influenced PV forecasts. Six variables were used as input vectors in this process to estimate the output power of the photovoltaic plant: low-level cloudiness, relative humidity of extraterrestrial insolation, normalized temperature, upper-level cloudiness, and mid-level cloudiness.

We compared the predicted values produced by the support vector machine and those produced with the conventional technique using the mean absolute error, mean absolute percent error, and the root means square error. The results revealed that the support vector machine algorithm offered accurate projections of photovoltaic energy production. Furthermore, the selection of internal parameters significantly impacts the PV output power. A good selection of support vector machine parameters is, therefore, a critical step in increasing the overall efficiency of the model. We did not well investigate the estimation of energy generated by the photovoltaic output power using the k-nearest neighbor machine learning algorithm.

Materials and Methods

Data Processing

We used the history of photovoltaic solar generation measurements to propose a forecast model. For the quality of the prediction-model-performance, the data must have possible quality. The data must be free of errors and disturbances caused by equipment and measurement sensor failures or events in the photovoltaic solar generation system or other unnatural causes that could affect the output power path. Errors and perturbations lead to outliers, discontinuities, and data gaps, compromising the model's fit and the quality of its predictions. There were applied filters for pre-processing data: (i) treatment of null values and (ii) filtering of overestimated records.

Forecast Model

We used the k-nearest neighbor (kNN) algorithm to develop the forecast model [11]. kNN uses distance functions to find a set of k samples closest to unknown samples. The k most similar instances closest to the current data point used a labeled dataset. As a result, the algorithm predicts how similar the recently received observations are to the training observation. During the learning phase, this algorithm maintains the complete training set. Unknown samples (i.e., new input data) have their labels (classes) compared to each instance in the training set, and by finding the mean of the response variables, we can predict them.

Regarding prediction, kNN is a good algorithm [12] since it uses local knowledge and highly adaptive behavior. However, one of the limitations of kNN is that a large amount of historical data is needed to build a model to search for the k nearest neighbor. When making predictions about regression problems, KNN will average the most similar

instances in the training dataset. The parameter k controls the size of the neighborhood. For example, if set to 1, predictions are made using the single training instance most similar to a given new pattern for which a prediction is requested. Common values for k are 3, 7, 11 and 21 [12]. Another important parameter is the distance measure, which controls how training data is stored and searched. The studies used Euclidean distance to calculate the distance between instances, which is good for numerical data with the same scale. Manhattan distance is good to use if its attributes differ in measurements or type.

Data Used

We used the dataset collected from the photovoltaic system [13], located on the campus of the University of Salento, in Monteroni di Lecce (LE), Apulia, Italy (40°19'32" 16N, 18°5'52" 44E) developed within the scope of the European project "7th Framework Program Building Energy Advanced Management Systems (BEAMS)". The collected data are related to the 960kW P photovoltaic system. We installed the photovoltaic modules in shelters used as parking lots. The first section of the system has 1,104 modules and an effective area of 1,733.3 m2, and the second has 1,896 modules and an effective area of 2,976.7 m2. It also has inverters for injecting the energy generated into the grid, an ambient temperature sensor, two other sets of sensors (temperature of the modules and global solar irradiation), one for each section of the system, and a SCADA system for the collection and storage of data. In this research, we used the following data sets: measurements of the University of Salento system for 21 months (from April 2012 to December 2013), covering measurements, on an average hourly basis, of the global solar irradiance in the two sections of panels and the total generation of the panels.

Results and Discussion

We used the cross-validation technique (10-fold cross-validation) to evaluate the computational model based on the kNN method for photovoltaic power prediction. We configured the model with k = 3, 5, 7, 9, 11, and 21. The distance measure used was the Euclidean distance since the numerical data present in the data set were on the same numerical scale.

The number of instances present in the original dataset was 11,919. After applying the filters in the pre-processing step, the number of instances was reduced to 9,426. Table 1 presents the relative absolute error and the root relative squared error in percentage for the different k parameters.

We observed that the best k was 21, with an error of 5.5% and 12.7%. Figure 1 shows the predicted and actual values of all 9,426 training cases using kNN. The y-axis projects values for each PV power, while the x-axis presents the actual values. The model follows the photovoltaic power prediction closely, although it presents variations.

Table 1. Forecast error.

k	Absolute error (%)	Squared error (%)
3	5.9	13.6
5	5.8	13.1
7	5.7	13
9	5.6	12.8
11	6	12.8
21	5.5	12.7

Figure 1. Diagram example.

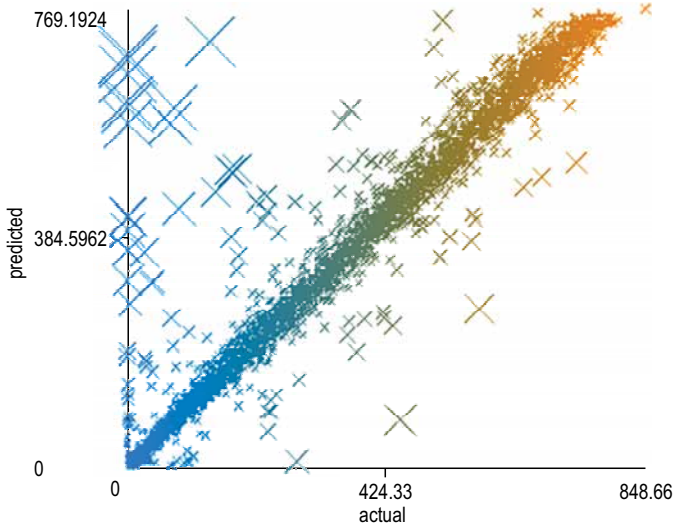

For the case of kNN, the algorithm searches in the feature space for the k closest samples depending on a predetermined distance. As a result, kNN is evaluated using the parameter k, implying that k is the key-setting parameter. So, based on the data set, the objective is to get the best value of k in the model.

Conclusion

Accurate power output prediction is critical for the operational planning of electrical power systems. In this study, machine learning estimated the energy generated by a solar photovoltaic system located in the Italian Mediterranean region of Italy. The results show a reasonable agreement between the actual and predicted values. This study implies that the machine learning technique, particularly the kNN, can be used to characterize other areas of the photovoltaic installation and other photovoltaic generators. Future research will analyze other databases to find appropriate indicators of merit. With this study, it may be possible to predict PV power using just a few small samples accurately.

Acknowledgments

The authors are grateful for the financial support of partner institutions SENAI CIMATEC and CHESF/ANEEL.

References

1. Fan J, Wu L, Zhang F, Cai H, Wang X, Lu X, Xiang Y, Evaluating the effect of air pollution on global and diffuse solar radiation prediction using support vector machine modeling based on sunshine duration and air temperature, Renewable and Sustainable Energy Reviews 2018;94:2090-4479.
2. Mas'ud A. Comparison of three machine learning models for the prediction of hourly PV output power in Saudi Arabia, Ain Shams Engineering Journal 2022;13:732-747.
3. Hemeida AM, El-Ahmar MH, El-Sayed AM, Hasanien HM, Alkhalaf S, Esmail MFC, Senjyu T. Optimum design of hybrid wind/PV energy system for remote area, Ain Shams Engineering Journal 2020;11:2090-4479.
4. IEA (2018), World Energy Outlook 2018, IEA, Paris https://www.iea.org/reports/world-energy-outlook-2018.
5. Graditi G, Ferlito S, Adinolfi G. Comparison of Photovoltaic plant power production prediction methods using a large measured dataset. Renew Energy 2016;90:513-519.
6. Hiyama T, Kitabayashi K. Neural network based estimation of maximum power generation from PV module using environmental information. IEEE Trans Energy Convers 1997;12(3):241-247.
7. Al-Amoudi A, Zhang L, Application of radial basis function networks for solar-array modelling and maximum power-point prediction. IEE Proc Gener Transm Distrib 2000;147(5):310.

8. Almonacid F, Rus C, Pérez-Higueras P, Hontoria L. Calculation of the energy provided by a PV generator. Comparative study: Conventional methods *vs*. artificial neural networks. Energy 2011;36(1):375-384.
9. Mellit A, Kalogirou SA. ANFIS-based modelling for photovoltaic power supply system: A case study. Renew Energy 2011;36(1):250-258.
10. Fonseca JGS, Oozeki T, Takashima T, et al. Use of support vector regression and numerically predicted cloudiness to forecast power output of a photovoltaic power plant in Kitakyushu, Japan. Prog Photovoltaics Res Appl 2012;20(7):874-882.
11. Cover T, Hart P. Nearest neighbor pattern classification. IEEE Trans Inf Theory 1967;13(1):21-27.
12. Al-Qahtani FH.Multivariate k-nearest neighbour regression for time series data — A novel algorithm for forecasting UK electricity demand. Proceedings of the International Joint Conference on Neural Networks 2013.
13. Malvoni M, De Giorgi MG, Congedo PM. Data on photovoltaic power forecasting models for Mediterranean climate. Data in Brief 2019;7(1):1639-1642.

Redesign of a Hydraulic Manifold in Additive Manufacturing for Application in a Cleaning and Inspection Robot

Luis Fellipe Lopez de Carvalho[1*], Luana Seixas Andril Araújo[1], Valter Estevão Beal[1], Rafael Tobio Claro[1], Juan Carlos Romero Albino[1]

[1]SENAI CIMATEC, Industrial Product Development; Salvador, Bahia, Brazil

A flexible joint riser inspection and cleaning robot must be small and powerful to perform its mission. Hydraulic units are commonly used in submerged operations for power. We designed a custom hydraulic unit as a robot. As the hydraulic manifold is complex, we developed it to be fabricated by additive manufacturing. The objective was to reduce the volume and mass of the hydraulic power unit. We achieved several computational analyzes and analytical methods to validate the designed concept. As a result, we obtained a more compact and lighter structure at the end of the process.

Keywords: Additive Manufacturing. Hydraulic Manifold. Selective Laser Melting. Structural Analysis. Dimensioning.

Introduction

With the advance of industry 4.0, additive manufacturing (AM) started to gain more space, and its use became common in several sectors. For Keller and Mendrickt (2015) [1], it occurrs mainly due to the possibility of producing parts in complex shapes that conventional manufacturing methods cannot obtain.

According to Aboulkhair and colleagues (2019) [2], the AM process has the potential to reduce the design-to-manufacture time of the part by simplifying the production steps (often, the final part is obtained without the need for manufacturing molds and machining process). In addition, there is a reduction in raw materials and materials utilized in components. It means that there is possible to generate more resistant and lighter parts.

In partnership with SENAI CIMATEC, Shell Brasil is developing a robot to clean and remove marine life from flexible joints of rigid risers on floating production platforms. One of the main components that allow the robot to perform its function is a hydraulic manifold, equipment whose function is to regulate the fluid flow between the pumps and actuators.

The original manifold is a multi-channel structure made of 6061-T6 aluminum, and it has a mass of 3.5 kg [Figure 1(A)]. In this part are coupled five directional valves, a relief valve, a pressure transmitter, a hydraulic accumulator, a motor-pump system, and an air spring [Figure 1(B)]. In addition, the structure was designed to support high loads due to the high power generated by the hydraulic system. A complete structure coupled with the manifold [Figure 1(C) and (D)], with a total height of 372.7 mm and approximately 13.10 kg. The internal channels through which the fluid flows have a diameter of 6 mm and operate under a maximum internal pressure of 60 bar.

Based on this problem, this work presents the redesign of the manifold using the benefits provided by additive manufacturing. As a result, the piece obtained is lighter and occupies a smaller volume than the original, supporting the same mechanical stresses.

Materials and Methods

Figure 2 summarizes the flowchart with the activities used to redesign the manifold.

We adopted an aluminum alloy with properties like the original model as a material. This choice

Received on 16 June 2022; revised 21 August 2022.
Address for correspondence: Luis Fellipe Lopez de Carvalho. Rua Coronel Durval Mattos, 826 - Costa Azul, Salvador - BA - Brazil. Zipcode: 41760-160. E-mail: fellipelopez78@gmail.com. DOI 10.34178/jbth.v5i3.223.

J Bioeng. Tech. Health 2022;5(3):173-179

Figure 1. Original manifold (A), original manifold assembly (B), structures attached to the manifold (C), and view of internal components (D).

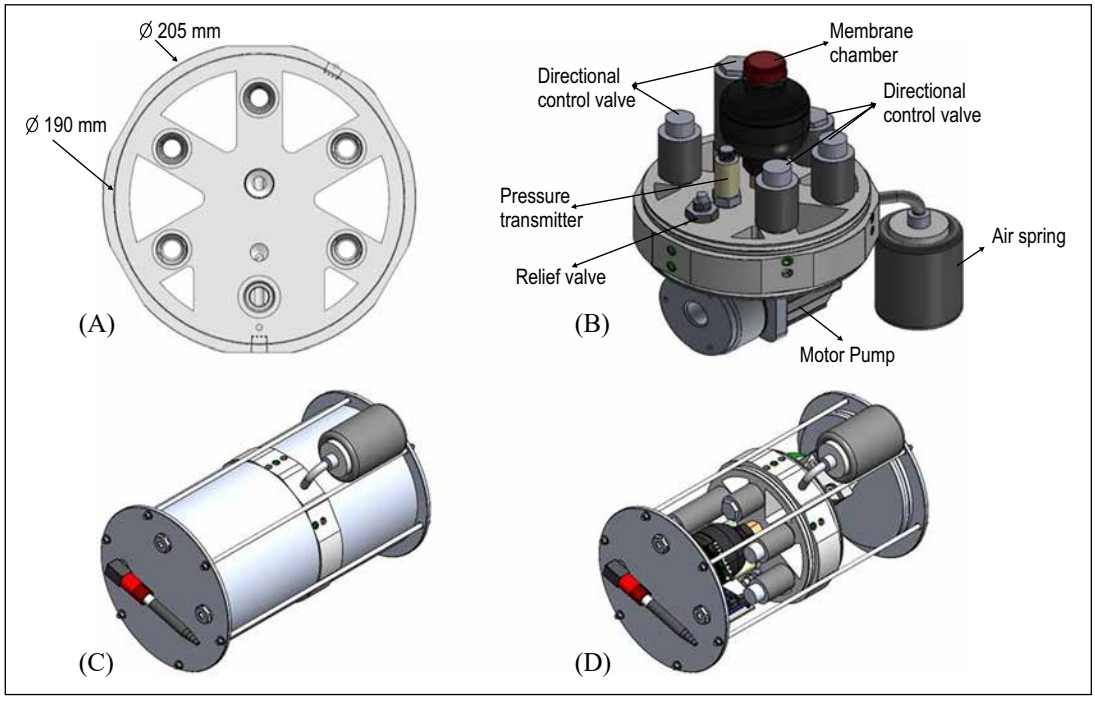

Figure 2. Activities' flowchart.

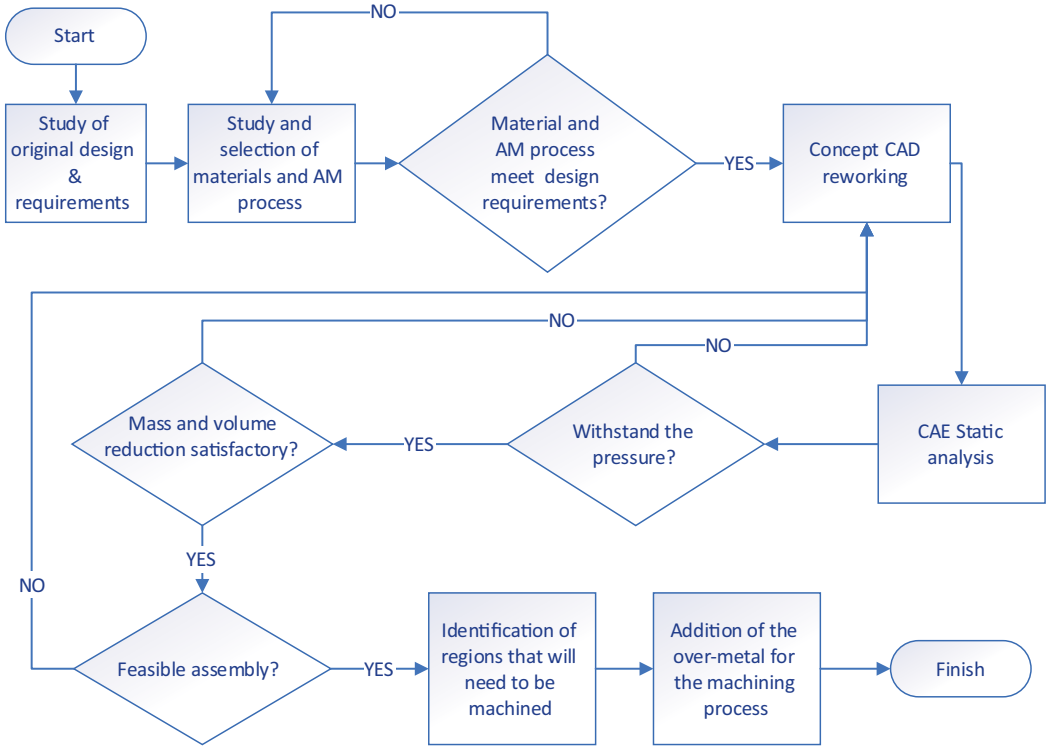

was based on the design requirements since the material support stresses would be high for a polymeric material. Thus, the selected alloy was AlSi10Mg, which has a low density and good corrosion resistance since the part will be submerged in the sea. Furthermore, according to Zygula and colleagues (2018) [3], this material has excellent moldability, low shrinkage, and low melting temperature, making it a good material for additive manufacturing.

The printing method was SLM (Selective Laser Melting). This process uses a high-energy laser beam to melt metal powder in a protective atmosphere, and the molten metal quickly solidifies. A three-dimensional component is eventually formed by repeating this procedure and overlaying it layer by layer. According to Zhang and colleagues (2018) [4], this technology is one of the most promising in the universe of additive manufacturing, as it produces parts with excellent quality and performance, in addition to being possible to reuse the metallic powder that was not cast, reducing the costs.

We used three software for the proposed concept: Solidworks for 3D modeling, Altair Inspire for static analysis and topological optimization, and Ansys for static analysis. Two software performed the analyzes to compare the results. We used the von Mises failure criterion to predict the onset of yielding. After developing the concept, we researched studies of stress concentrators and dimensional calculations. To calculate the diameter of the channels, we consulted Norton (2013) [5] and Shigley (2005) [6] to find the hoop (σθ) and radial (σr) stresses in thick-walled cylinders. In addition, we consulted ASME [7] for the maximum allowable stress. With the concept defined, it was also necessary to think about the correct order of assembly of the components, ensuring the feasibility of the assembly. Finally, Kamurudin and colleagues (2016) [8] adopted dimensional precision to add the extra metal. The final part will need to go through the machining process for threading and the surface finish required for some areas of the part.

Material Characterization

The alloy adopted is supplied by the company SLM Solution [9] and has the following chemical composition: 9%-11% Si, 0.55% Fe, 0.05% Cu, 0.45% Mn, 0.20%-0.45% Mg, 0.10% Zn, 0.15% Ti, 0.05% Ni, 0.05% Pb, 0.05% Sn, 0.15% other substances and the remainder aluminum. We used data referring to alloy particles of 60 μm with a laser power of 700 W. After printing, the manufacturer recommends heat treatment to relieve residual stresses by heating the part at 300 °C for 2 hours. Table 1 presents the mechanical properties of the alloy used. In addition, the SLM process has a print rate of 67.9 cm³/h.

Table 1. Mechanical properties of AlSi10Mg [9]

Information	Data
Density (g/cm³)	2.67
Tensile strength (MPa)	261
Yield strength (MPa)	141
Young's modulus (GPa)	59

Dimensioning of the Internal Manifold Channels

For dimensioning the channels, the hoop (σθ) and radial (σr) stresses were calculated by the following equations [5, 6]:

$$\sigma_\theta = \frac{p_i r*_i{}^2 p-_o r*_o{}^2}{r_o{}^2 r-_i{}^2} + \frac{r_i{}^2 r*_o{}^2 p(*_i p-_o)}{r^2 r(*_o{}^2 r-_i{}^2)} \quad (1)$$

$$\sigma_r = \frac{p_i r*_i{}^2 p-_o r*_o{}^2}{r_o{}^2 r-_i{}^2} - \frac{r_i{}^2 r*_o{}^2 p(*_i p-_o)}{r^2 r(*_o{}^2 r-_i{}^2)} \quad (2)$$

(pi and po represent the internal and external pressure, ro is the external radius, ri is the internal radius, and r is the radial coordinate).

Results and Discussion

Manifold Design

The redesign of the original manifold (Figure 1) sought to reduce mass and height. Therefore, we redesigned the proposed structure entirely for

mass reduction. Only functional structures were kept, like the internal channels through which the fluid will flow, the walls of the structure, the valve cavities, the pump support, and hydraulic actuators (Figure 3).

The stresses in the most critical inner channel, with dimensions ri = 3 mm, ro = 4.75 mm, pi = 60 bar, and po = 5 bar, were calculated according to Eqs. 1 and 2 (Figure 4).

The maximum von Mises stress obtained in the channels was 16 MPa. This value was compared with the allowable stress according to ASME [7], whose value is 74.5 MPa. As a result, the stresses in the channels are below the allowed limit. In addition, to support the ducts during the printing process and also to reduce the stress concentration, the fillets suggested by Morgenbrod (Walter D. Pilkey and Deborah F. Pilkey, 2008) [10] were used in the geometry changes arising from the connections of the channels with the cavities. This fillet type is often used on heavy shafts to avoid high stress. There was an increase in the internal diameter of the manifold, from 190 mm to 198 mm, to reduce the structure's height. It allows a better reorganization

Figure 3. Proposed manifold concept (A) and its assembly with the main components (B).

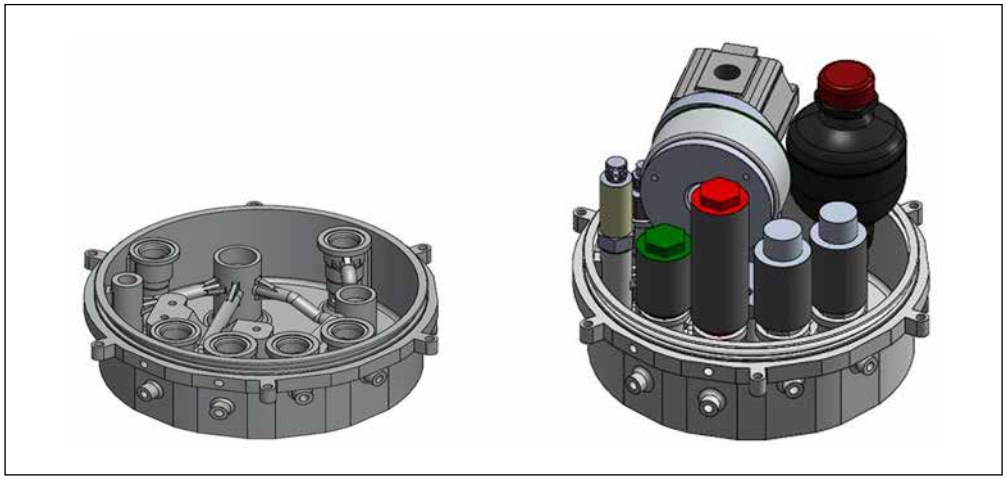

Figure 4. Hoop stress (A) and Radial stress (B) are based on the channel radius.

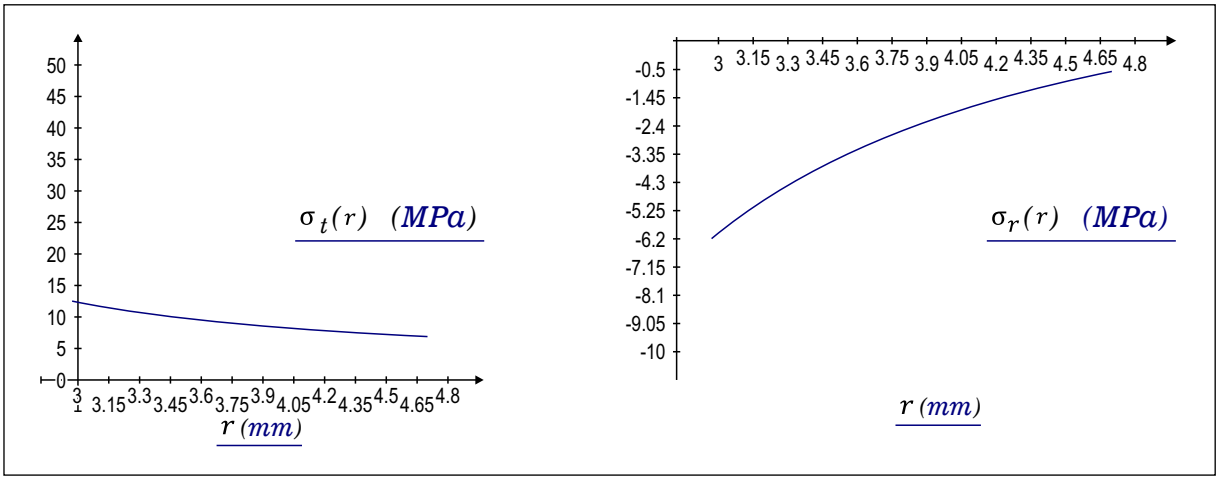

of the components, leaving them on only one side of the structure and eliminating the lower tray and cylinder. In addition, the tie rods now connect directly to the manifold (Figure 5).

We executed a static analysis of the manifold, considering an operating pressure of 60 bar inside the channels. Furthermore, due to the presence of the "air spring", whose function is to equalize the internal pressure of the manifold with the external pressure (of the water depth of 40 m), an internal and external pressure of 5 bar was adopted in the manifold. As a result, the manifold had a safety coefficient of 1.2, using von Mises as a failure criterion for the onset of yielding. Figure 6 shows the result of the static analysis.

Table 2 compares the original manifold and the manifold proposed in this work. If we consider the assembly complete, we obtained a 30% reduction in height and a 39% reduction in mass with the proposed manifold.

Machining

After printing the part, it is still necessary to carry out some machining processes to generate the necessary threads and give the recommended surface

Figure 5. New assembly structure (view of internal components) (A) and covered (B).

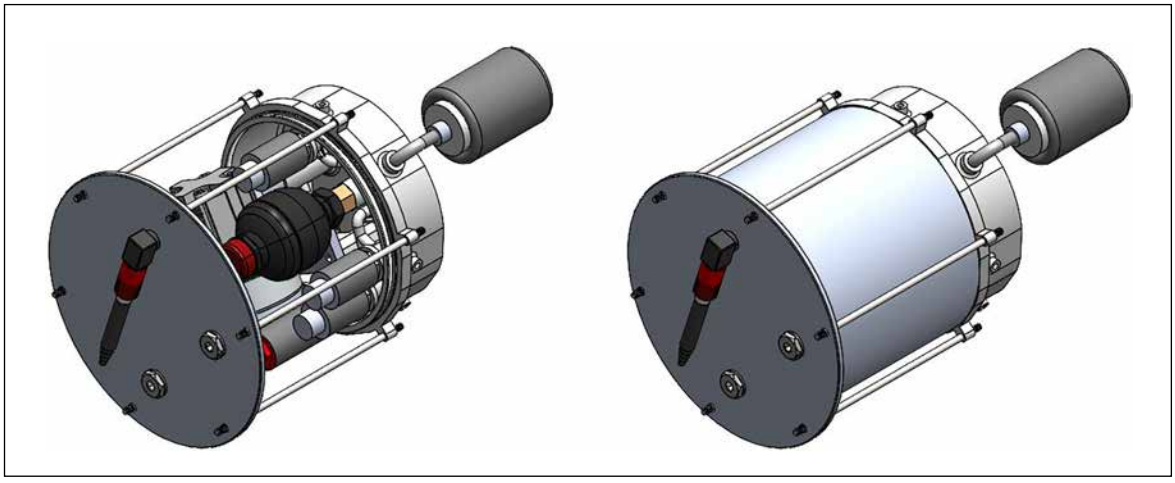

Figure 6. Result of static analysis of the manifold (von Mises stress).

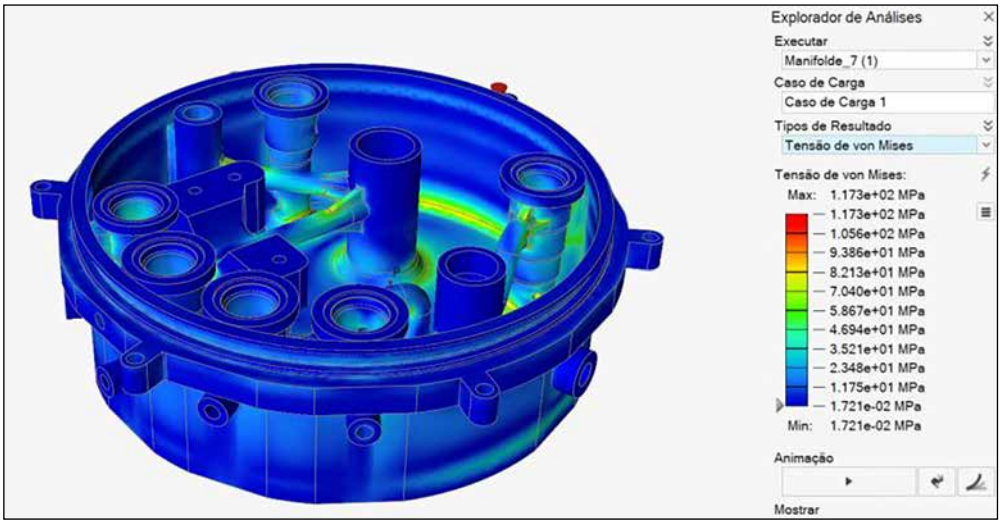

Table 2. Models comparison.

Information	Original structure	New AM concept
Manifold Mass (kg)	3.5	1.76
Volume (cm^3)	Not applicable	659
Complete structure mass (kg)	13.10	8
Complete structure height (mm)	372.7	259.0
Manufacturing time (hr)	Not applicable	9.7

finish for each specific region. For this reason, we tried to add an over-metal in these regions. The over-metal was calculated based on the dimensional accuracy of the SLM printing process and added a safety value, thus ensuring the existence of the amount of material needed for the part to be machined. According to Kamurudin et al. (2016) [8], for cylinders between 10 and 5 millimeters in diameter, there is a variation between 1.3% and 2%. Therefore, a 2.5% diameter surplus was adopted in the regions undergoing the machining process.

Conclusions

The new manifold withstood the operating demands well, reducing the structure's mass and making it more compact, representing a significant reduction in mass and height. In addition, the redesign reduced the number of components involved in the structure. However, the reduction of mass and volume is not that significant compared to the complete robot. However, this work can be the first step to redesigning other structural components in MA and obtaining more significant results. On the other hand, the assembly of the components of the new manifold became more complex, having to obey a particular order to guarantee the correct fixation of all the elements. However, this difficulty in the assembly does not represent a significant disadvantage. Another disadvantage, this one significant, is the cost of manufacturing the structure. By the traditional method (machining), the cost per part was around 1,500 dollars. With the AM, the cost is around 1,500 to 2,000 dollars, and it will still be necessary to carry out some machining processes to generate threads and surface finish. The following steps in the project are to obtain more information about the material to perform fatigue analysis on the part, ensuring its good functioning and estimating its lifetime. Later, we expect to print the manifold and perform tests on the prototype.

Acknowledgments

The authors thank the support of HP Brasil Indústria e Comércio de Equipamentos Eletrônicos Ltda, SENAI CIMATEC, and SHELL do Brasil. This project was funded by HP Brasil using resources based on Law #8.248 of 1982 (Informatics Law).

References

1. Keller P, Mendricky R. Parameters influencing the precision of SLM production. MM Science Journal 2015(out):705-710.
2 Aboulkhair TN. 3D printing of aluminium alloys: Additive manufacturing of aluminium alloys using selective laser melting. Progress in Materials Science 2019;106(Dec).
3. Zygula K, Nosek B, Pasiowiec H, Szysiak N. Mechanical properties and microstructure of AlSi10Mg alloy obtained by casting and SLM technique. World Scientific News 2018(July):462-572.
4. Zhang J. A review of selective laser melting of aluminum alloys: Processing, microstructure, property and developing trend. Journal Of Materials Science & Technology 2019(Feb):270-284.
5. Norton RL. Projeto de Máquinas: uma abordagem integrada. 4. ed. Porto Alegre: Bookman, 2013.
6. Shigley JE, Mischke CR, Budynas RG. Projeto de Engenharia Mecânica 7. ed. Porto Alegre: Bookman, 2005.

7. The American Society of Mechanical Engineers. Boiler and pressure vessel code: Section II, Part D: Properties. New York: The American Society of Mechanical Engineers, 2019.
8. Kamarudin K, Wahab MS, Shayfull Z, Ahmed A, Raus AA. Dimensional accuracy and surface roughness analysis for AlSi10Mg produced by selective laser melting (SLM). MATEC Web of Conferences, 2016.
9. SLM Solutions. Al-Alloy AISi10Mg. Material Data Sheet. Available: https://www.slm-solutions.com/fileadmin/Content/Powder/MDS/MDS_Al-Alloy_AlSi10Mg_0221.pdf; Last access: 15/september/2021.
10. Pilkey WD, Pilkey DF. Peterson's Stress Concentration Factors. 3. ed. United States Of America: John Wiley & Sons, 2007.

Experimental Study of Oil Deposition Using a Deposition Simulator (HLPS - Hot Liquid Process Simulator)

Hugo Gomes D'Amato Villardi[1*], Lucas Cunha Orrico[1], Ana Lucia Barbosa de Souza[1], Antonio Rimaci Miguel Junior[1], Fernando Luiz Pellegrini Pessoa[1]

[1]SENAI CIMATEC University Center, Chemistry Department; Salvador, Bahia, Brazil

Fouling in heat exchangers is a recurring and costly problem for oil refineries. However, the phenomenon is complex and requires experimental evaluation, as oils have varied compositions. In the present study, analyzes were performed in the laboratory using a deposition simulator (HLPS - Hot Liquid Process Simulator). We performed the test with a sample of crude oil. In this test, the deposition was small, which could occur due to the characteristic of the oil.
Keywords: Oil. Heat Exchanger. Fouling. HLPS.

Introduction

Fuels are still the main responsible for the world's energy Generation, and with the advancement and growth of industry and commerce, there is more and more demand for energy. This need for energy, and therefore derivatives, makes it necessary to increase their production. For this, it is necessary to refine more and more oil and, consequently, the unit operations involved, including the transfer of heat in exchangers. An important phenomenon in the operation of heat exchangers is fouling. The deposition of solid material on the surface of the equipment presented fouling. This deposition can occur as a result of the phase change that arises from temperature differences between the surface and the fluid (deposition by crystallization), by chemical reactions on surfaces (deposition by chemical reaction), or even the growth of organisms on the surface (biodeposition). It is an essential phenomenon because the deposited solid material can restrict the cross-sectional area for fluid flow, causing an increase in pressure drop. In addition, this material acts as a resistance to heat transfer, thus limiting heat recovery and increasing energy and cleaning costs [1]. Fouling rates are complex functions of oil composition, temperature, velocity, and particle content [2], simulation, and evaluate the deposition in heat exchangers.

We built mathematical models with researched information that associate the existing conditions and the deposit rate in oil streams. The performance of a comparative analysis of the prediction performance of models against deposition data sets, plus laboratory availability for experiments, was crucial for the selection of the concept for simulation in HLPS.

Materials and Methods

Relating the properties of crude oil and diesel with the conditions provided by the HLPS apparatus, we based the experimental planning

Figure 1. HLPS equipment.

Received on 26 June 2022; revised 31 August 2022.
Address for correspondence: Hugo Gomes D'Amato Villardi. Av. Orlando Gomes, 1845 - Piatã, Salvador - BA- Brazil. Zipcode: 41650-010. E-mail: hugo.villardi@fbter.org.br. DOI 10.34178/jbth.v5i3.224.

J Bioeng. Tech. Health 2022;5(3):180-184

on variables: flow, time, and tube temperature; aiming to develop methods of indicating the period of maintenance of the process in function of the incrustation created by the deposit. The technique used to assess the influence of some conditions on a given event allows us to define which quantity and conditions of specific parameters can satisfy two significant objectives: the most significant possible statistical precision in the response and the lowest cost. Table 1 shows the conditions used in the tests carried out with diesel and crude oil.

Experimental

The oil is in the supply and agitation reservoir, with the fluid pumped to the tube-in-shell heat exchanger, a single-pass heated, annular section electric heating resistance system. The fluid is destined for a receiving reservoir similar to the inlet. The parts that make up the heat exchanger and the equipment supply lines must be sealed according to their inputs, such as o-ring, washers, grease, and other connections (Figures 2 and 3). Leakage tests were conducted under atmospheric pressure of 10 bar with Nitrogen gas.

To start the experiment, we adjusted the parameters in the programmable logic controller (PLC) according to the experimental planning (Table 1).

We monitored the experiment's performance on the control panel screen for data collection and analysis for the mathematical modeling of deposition (Rf) (Figure 4).

We removed the "hot finger" to investigate the oil deposit through the difference in weight before and after the experiment. The HLPS equipment uses an annular test section with a heated 60 mm length calibrated at 38 mm for the deposition

Figure 2. Adding oil to the reservoir.

Figure 3. Programmable Logic Controller (PLC).

Table 1. Crude oil deposition test conditions in HLPS.

Test	Twall (ºC)	Flow (mL/min)	Time (h)	T_{inlet} (ºC)	T_{bulk} (ºC)	T_{oulet} (ºC)	$P_{average}$ (bar)
PC	292.74	18	1.39	150.41	182.09	213.78	11.93

Figure 4. Control panel.

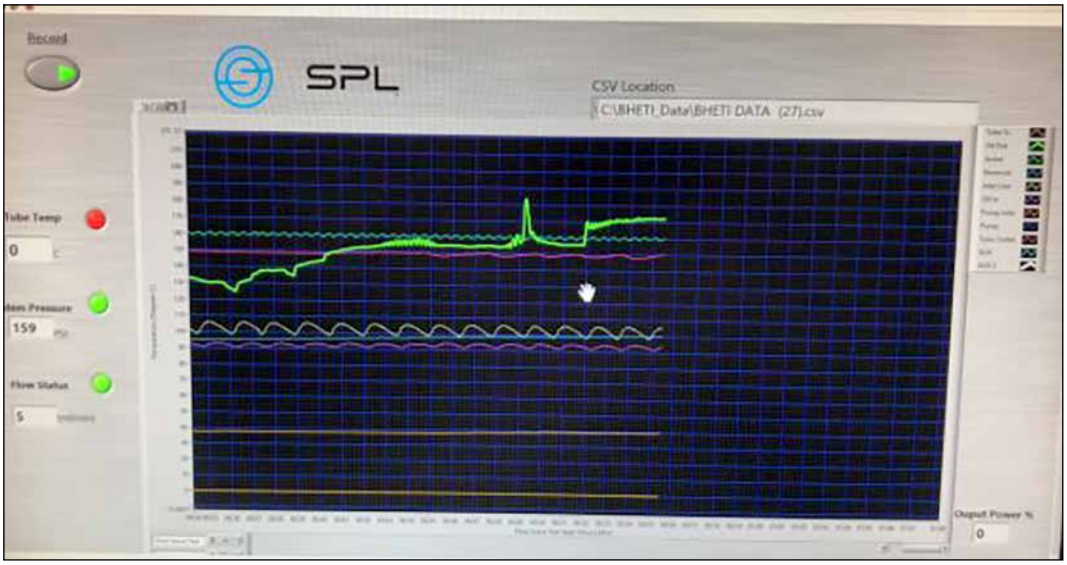

phenomenon. Figure 5 shows the deposition of heated oil in the annular section.

Figure 5. The hot fluid reservoir region.

For new tests, the equipment and lines are disconnected and washed with heptane, toluene, or hexane solvent in a hood with an exhaust.

Results and Discussion

We did the calculations considering the deposition in the hull and the tube. The literature demonstrates several studies of predictive models. Nevertheless, we based our study on some models. The outlet temperature is higher than the inlet temperature, considering the tube temperature in the condition calibrated for testing. We based the experimental Rf calculations on the work by Trafczynsk and colleagues [3] (Equations 1-6).

Uf and other physical properties were calculated with flow and temperature values measured by the control panel every second. In the mathematical model by Yeap and colleagues

Equations 1-6.

$$U_c = \frac{Q_t}{A\Delta T_{lm}} = \frac{mC_p\Delta T}{Af_t\Delta T_{lm}} \quad (1)$$

Tempo (>0)

$$U_f = \frac{Q_t}{A\Delta T_{lm}} = \frac{mC_p\Delta T}{Af_t\Delta T_{lm}} \quad (2)$$

$$\Delta T_{lm} = \frac{(TF_S - TF_E)}{ln(TF_S - TF_E)} \quad (3)$$

$$R_f = \frac{1}{U_f} - \frac{1}{U_c} \quad (4)$$

$$f_t = 0{,}014 + \frac{1{,}056}{Re_t^{0,42}} \quad (5)$$

$$Re = \frac{Du\rho}{\mu} \quad (6)$$

[4], the physical properties are determined by the proposed correlation (Equations 7-12), where the bulk and wall temperatures are considered. Therefore, the Uf calculation used the average temperature and Q [4].

Figure 6 presents the results of the thermal behavior of the input, output, wall, and tube heating power obtained.Figure 7 shows the calculated Rf values.

The results show the linear and continuous behavior of the exit and deposition temperatures, confirming the non-deposition in the tested conditions. Data close to 1,000 seconds and 2,000 seconds represent a cooling of the equipment, which means unforeseen programming of the controllers. However, this has already been identified and corrected by the team. The critical point in this work is calculating the Rf and evaluating the deposition. As the equipment allows fine and low flow control, it is possible to carry out tests in hours representing months in the refinery. Thus, the next step is to conduct an

Equations 7-12.

$$\rho = 1234{,}18 - 5{,}46API - 0{,}300T_b - 0{,}367T_p \quad (7)$$

$$\lambda = 0{,}1314 + 0{,}000727API - 0{,}0000321T_b - 0{,}0000392T_p \quad (8)$$

$$C_p = 342{,}57 + 11{,}273API + 1{,}82T_b + 2{,}227T_p \quad (9)$$

$$log_{10}^{\vartheta} = \frac{b_{A6}}{\left(1+\left((0{,}45T_b+0{,}55T_p)-310{,}93\right)/310{,}93\right)^{b_{A7}}-0{,}8696} \quad (10)$$

$$b_{A6} = log_{10}\vartheta_{37{,}78^{o}C} + 0{,}8696 \quad (11)$$

$$b_{A7} = 0{,}28008b_{A6} + 1{,}6180 \quad (12)$$

Figure 6 . Thermal behavior of the HLPS simulation (crude oil, T wall = 292.74ºC and pressure = 11.93 bar).

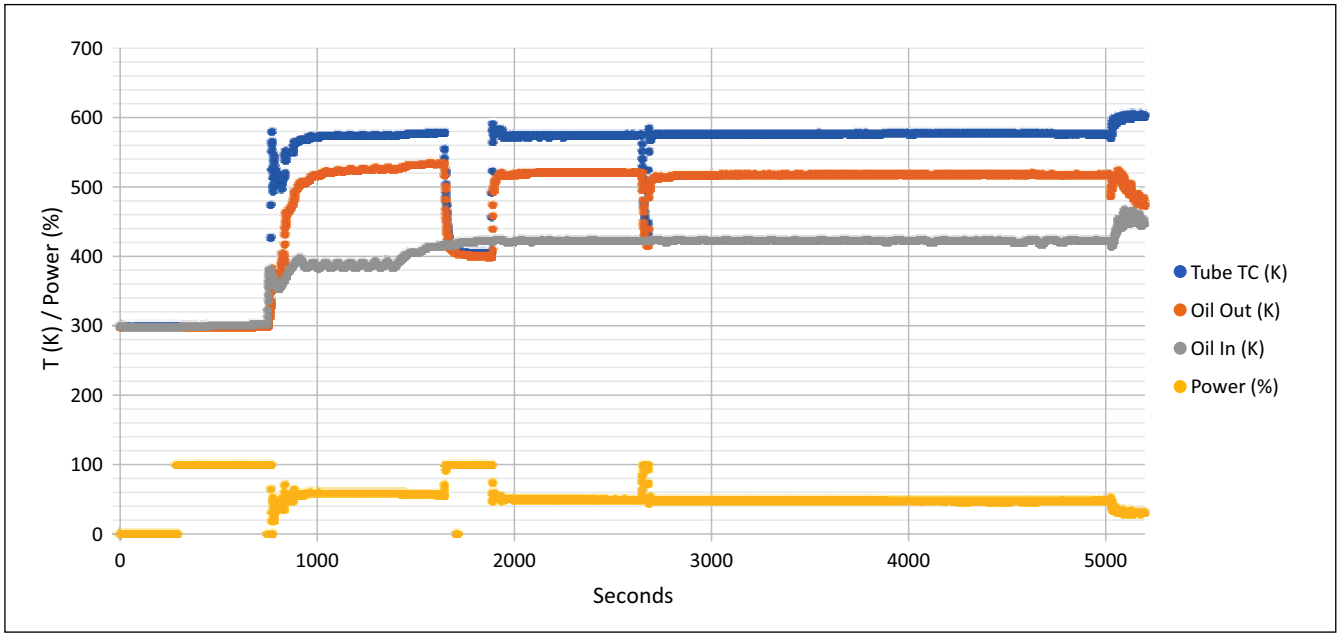

Figure 7. Behavior of the Rf measured experimentally (crude oil, 292.74ºC Twall, and 11.93 bar pressure).

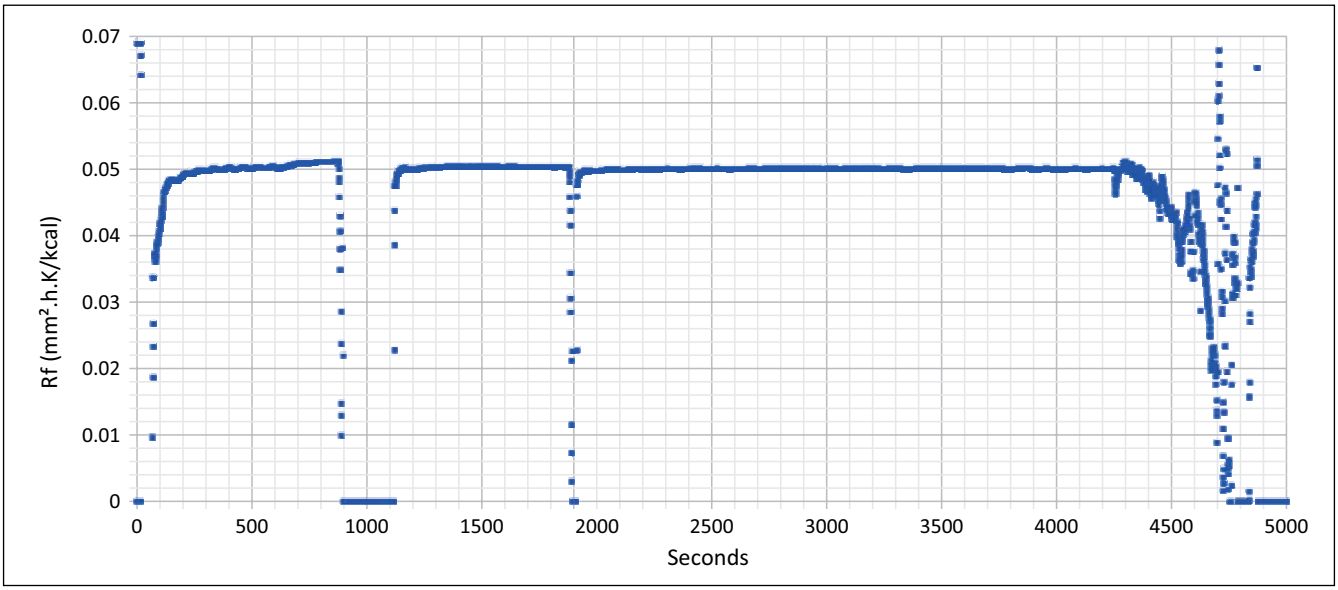

exploratory study with the essential parameters and obtain a better understanding of the phenomenon.

Conclusion

The study evaluated the experiment's method concerning threshold models in predicting deposition in heat exchangers. The data shows that the need for the equipment is measured successfully. However, tests in other conditions or with denser samples are necessary to obtain deposition data. In addition, it is necessary to evaluate the influence of correlations, which consider fluid conditions, such as temperature and density, on the accuracy of the data. Thus, the need for improvements and sequencing in the study is clear, seeking a greater understanding of the deposition behavior of this oil.

Acknowledgments

The authors thank CENPES/PETROBRAS for funding the research and SENAI CIMATEC for the availability of the structure for its developmentt.

References

1. Pental JK. Design and commissioning of a crude oil fouling facility. 2011(October).
2. Watkinson AP. Comparison of crude oil fouling using two different probes. Heat Exch. Fouling Clean. Fundam. Appl. 2003.
3. Trafczynski M, Markowski M, Urbaniec K, Trzcinski P, Alabrudzinski S, Suchecki W. Estimation of thermal effects of fouling growth for application in the scheduling of heat exchangers cleaning," Appl. Therm. Eng. 2021;182(Jan). Doi: 10.1016/j.applthermaleng.2020.116103.
4. Yeap BL, Wilson DI, Polley GT, Pugh SJ. Mitigation of crude oil refinery heat exchanger. Chem. Eng. 2004;82(January):53–71.

Selection of Internet of Things Based Communication Networks for Onshore Oil Field Monitoring

Amanda Bandeira Aragão Rigaud Lima[1*], Danielle Mascarenhas dos Santos[1], João Vitor Silva Mendes[1], Adeilson de Sousa Silva[1], Herman Augusto Lepikson[1]

[1]SENAI CIMATEC University Center; Salvador, Bahia Brazil

Onshore oil fields usually operate remotely without continuous human assistance and communication facilities. Oil transfer from the wells to the separation and storage tanks usually occurs via pipelines in these fields. This whole system is prone to failures with significant and unpredictable environmental impacts. Therefore, properly monitoring this production system is vital to mitigate relevant problems such as leakages. This paper presents a comparative evaluation of the leading candidate communication networks for this application on onshore oil field monitoring for potential leaks. Among the analyzed technologies, LPWANS, DigiMesh, and CBRS stand out.

Keywords: Internet of Things. Network. Communication.

Introduction

In Brazil, onshore oil production refers to mature and marginal fields. The vast majority of these fields are in inland regions, mainly in the Northeast. These areas lack infrastructures such as roads, electricity, telephone, and data network [1]. Information transmission in this environment is challenging. Therefore, any feasible solution shall be based on wireless communication network, and its architecture needs to be compatible with the specificities of the environment and the kind of data package to be transferred.

Developing a network depends on the analysis of latency, transfer rate, reliability, range, whether the network is licensed or not, coverage, scalability, and energy consumption, to choose a better configuration that meets the established requirements for the application [2].

Oil fields are remote environments, so developing a remote wireless network is necessary, and real-time networking is paramount. The network latency is the response time to the stimulus. The latency needs to be as low as possible to achieve real-time communication. [3,4]. It is necessary to know the packet size for transmission to send the message, and it depends on the data generated by the selected sensor. The more complex the message, the higher the transfer rate needed. Bandwidth is directly proportional to the concept of transfer rate [5,4].

Monitoring onshore oil fields aim to reduce the number of failures, so it is necessary to be sure that the message will arrive, represented by reliability, which is usually higher when the network bandwidth is licensed. Paying for the spectrum, there is a guarantee of service, but when it is not licensed, it becomes susceptible to interference or even lack of prioritization. In addition, the pipelines in the oil field are extensive, making it necessary to use a high-range network and affecting the cost of implementation because the longer the network range, the fewer repeaters are required.

The licensed network is recommended for data security, but it has an additional cost for licensing. Since the described environment has inadequate infrastructure, it becomes impractical to use most networks for not presenting coverage in the application area of the project. For network expansion, it is necessary to consider scalability [6]. It is necessary to analyze energy consumption to reduce expenses as much as possible since a high-energy expenditure will result in high costs.

Received on 13 June 2022; revised 28 August 2022.

Address for correspondence: Amanda Bandeira Aragão Rigaud Lima. Praça Igaratinga, 206, Cond. Monte Belo, Ed. Vista Bela, 1102, Pituba. Zipcode:41.830-290. E-mail: limaamanda285@gmail.com. DOI 10.34178/jbth.v5i3.225.

J Bioeng. Tech. Health 2022;5(3):185-189

This paper aims to evaluate the leading candidate communication networks for onshore oilfield monitoring applications for potential leaks. The technologies analyzed are LPWANS, DigiMesh, and CBRS.

Wireless Network

Radio wave networks make it possible to develop better equipment related to wireless technologies [7]. The wireless communication network became popular because it promotes portability and mobility to the user since it eliminates the use of cables. The rise of the IoT concept accentuated the relevance of wireless networks. Despite the advantages of this model, the network can have disadvantages if implemented or managed incorrectly, resulting in network problems [8].

It is possible to divide wireless communication into five categories: Private Radio, LPWAN, (Low-Power Wide-Area Network), Cellular Network, LAN (Local Area Network), and PAN (Personal Area Network). DigiMesh and CBRS (Citizens Broadband Radio Service) network operating in the Private Radio Frequency. Figure 1 shows their characteristics in range and power consumption.

LPWAN

LPWAN is a communication system focused on IoT featuring three different communication protocols, NB-IoT, Sigfox, and LoRaWAN, each of which has its particularities and different applications. As described by the name, LPWAN features high area coverage, high network range, low power consumption, and low bandwidth, so only sending small packets is possible [9,10].

NB-IoT

NB-IoT (Narrow Band-Internet of Things) is the only LPWAN technology that features a licensed network. 3GPP (3rd Generation Partnership Project), technology based on the LTE network. It is known for its narrowband and cellular network performance. It has a maximum transfer rate of 200 Kbps and can send 1600 bytes per packet [2]. Furthermore, it is real-time because it has a latency of 0.02 seconds. Moreover, it has a long battery life (ten years) because it does not stay connected to the cellular network, connecting just when activated [11]. Furthermore, its range in rural areas is up to 10 km. However, towers/ antennas are essential for network operation, meaning that in areas with inadequate infrastructures, such as some interiors, it is difficult to deploy an NB-IoT system [12].

Sigfox

Ultra-narrow bandwidth characterized the Sigfox network, which makes it more resilient to interference than the LoRaWAN network. In addition, the technology developed a battery to have a life of 10 years because it is not connected all the time, but the battery only lasts 5 to 7 years. The WND'S Business Develop Manager also stated that it is possible to set up a base station in remote areas with no connection, indispensable only power, and internet, and use a solar panel, as the internet does not need to be fast [13]. It has the advantage that it is possible to export the network without additional costs [13].However, it is not in real-time; the latency of the product is 10 seconds. There is a maximum number of daily transmissions depending on the package purchased; the simplest is three daily sends, which are paid by service. Due to the low transfer rate of 100 bps and maximum sending of 12 bytes [2], it has a longer packet transmission time, increasing power consumption. It ranges from up to 50 km in rural areas [13].

LoRaWAN

The LoRaWAN protocol makes use of Radio-Frequency LoRa technology [12]. One of its advantages is that it can be developed as a private network. However, the network makes use of a shared spectrum, receiving more self-interference,

Figure 1. Range and power consumption of network categories.

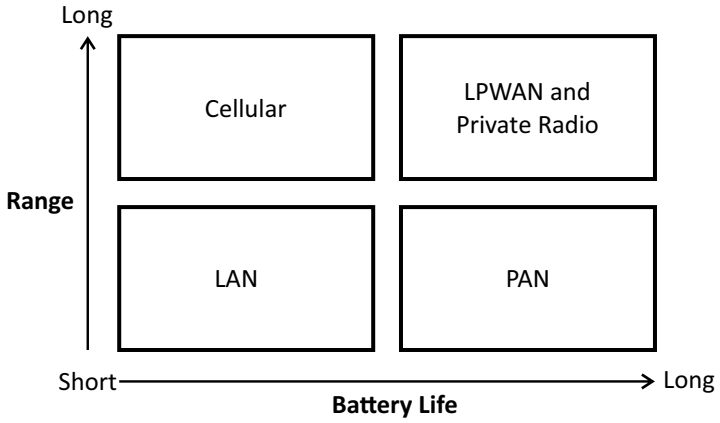

which ends up limiting the scalability of the network [14,15]. In addition, it connects in two different ways; firstly, access keys are generated for each use, increasing the network's security but increasing network complexity. The second way is without the use of access keys [13]. The transfer rate is 50 Kbps, and the latency of this network is 5 seconds. There is no daily packet limit, but each packet must contain a maximum of 243 bytes [2]. The range of the network is approximately 15 Km in rural areas, and there is no coverage in remote locations [15].

DigiMesh

The module analyzed in this paper is the Digi XBee-Pro 900HP-RF Module. The technology is related to Mesh Networks, which create a wireless mesh network, and perform multiple hopping, making possible communication of all devices in the network, making the network highly scalable [16]. Furthermore, as nodes send packets to other nodes, they act as "routers" [7]. The DigiMesh network presents a latency of approximately 0.035 seconds, and its power consumption is low since it presents a hibernation mode, consuming 2.5 microamps. However, during the reception, 29 microamps, and packet transmission, it consumes up to 120 microamps [17]. However, this network does not provide coverage in remote locations [17]. The lack of licensed network results in information vulnerability [18], and the communication's transfer rate changes according to the range of the network and the environment where it is being applied (Table 1).

CBRS

CBRS is a network developed for 'military' use and can use licensed radio frequencies. Its latency is 0.02 seconds, but military activity will have priority in the network, followed by the licensed networks and, lastly, the unlicensed ones [19]. In rural areas, it presents a range of ≤16 km. It has coverage in remote areas and is cheaper than in urban areas due to its proportionality with population density [20]. The licensed spectrum refers to the LTE radio interface, and the network differentiator is in the spectrum distribution. Leaving the SAS (Spectrum Allocation Server) responsible for allocating from

Table 1. DigiMesh operating characteristics.

	Indoor	**Indoor**	**Outdoor**	**Outdoor**
Range	610m	305m	15.5Km	6.5Km
Transfer rate	10Kbps	200Kbps	10Kbps	200Kbps

the calculation of RF density (Radio Frequency) [20]. The CBRS network has a throughput attribute of 1Mbps [21], which is an average bandwidth. The power consumption of this system is 47 dB [22].

Materials and Methods

The research is an explanatory literature review of Google Academic and IEEE Xplore periodical articles. It aims to assist in the choice of communication networks for monitoring onshore oil fields and performing analysis to simplify the network's choice.

Results and Discussion

After knowing each network individually and analyzing Table 2, it becomes possible to make a conscious choice of the network that will be acquired. Sometimes, there will not be a network that fits all parameters, so it is essential to use two or more types to approximate the required standard.

By observing the table, it becomes clear that LPWAN and the DigiMesh network do not have coverage in remote regions, which makes their application in the oil fields difficult. Sigfox, LoRaWAN, and DigiMesh networks are not licensed, compromising the user's data security. Sigfox has the lowest data transfer rate, restricting packet size. The low scalability of LoRaWAN makes it hard to grow the system. The energy consumption is low for all the networks. However, LoRAWAN's spectrum is susceptible to interference, which compromises the system's reliability. Therefore, the CBRS and NB-IoT are configured with the lowest latency, transferring data in real time. Ultimately, the more extensive range is CBRS. For connecting, NB-IoT needs a previous antenna to act in the cellular network. The LPWANs have many positive aspects, such as high bandwidth, low latency, licensed network, low power consumption, and high transfer rate. However, it lacks coverage in areas that lack electricity and internet. CBRS network's primary use is military, and it is unlikely to be applied in another spectrum, but when this happens, the cellular network is employed. However, it results in difficult usability in the project due to the need for operation in remote fields.

Conclusion

After analyzing the information in this article, it was possible to conclude that the perfect fit does not exist, but some points are worth recording. The Sigfox has the best range; however, it has a low transfer rate. The NB-IoT is licensed and has lower latency, higher reliability, and data transfer rate, although it does not have coverage in remote areas. DigiMesh network is famous for scalability and the facility of the installation, also having a high transfer rate, but is not reliable and licensed. On

Table 2. Comparison of the wireless network categories.

	NB-IoT	Sigfox	LoRaWAN	DigiMesh	CBRS
Rural area range	10 Km	50 Km	15 Km	15,5 Km	16 Km
Coverage in remote areas	No	Possible	No	No	Yes/No
Reliability	High	Medium	Medium	Medium	Medium
Energy Consumption	Low	Low	Medium	Low	Low
Scalability	Medium	Medium	Low	High	High
Latency	0.02 s	10 s	5 s	0.035 s	0.02 s
License	Yes	No	No	No	Yes/No
Transfer rate	200 Kbps	100 Kbps	50 Kbps	200 Kbps	1 Mbps

the other hand, LoRaWAN has the lowest cost for implementation and a good range; nevertheless, this network is susceptible to interference at the spectrum. Finally, CBRS has the highest range, reliability, scalability, and lowest latency. The only factor that is not good is weak resilience.

Acknowledgments

To CNPq and ANP PRH Program for the grants, to the Competence Center in Advanced Technologies and Competence Center in Onshore Solutions for the support.

References

1. Mendes APA, et al. Produção de Petróleo Terrestre no Brasil. Disponível em: <https://web.bndes.gov.br/bib/jspui/bitstream/1408/16962/3/PRArt214594_Producaode pretroleo terrestre no Brasil_P_BD.pdf>. Acesso em: 26 jan. 2021.
2. Mekki K, et al. Overview of cellular LPWAN technologies for IoT deployment: Sigfox, LoRaWAN, and NB-IoT. In: 2018 ieee international conference on pervasive computing and communications workshops (percom workshops). IEEE, 2018. p. 197-202.
3. Minha Conexão. Entenda o que é a Latência e sua influência na conexão com a internet. 9 April. 2020. Available at: <https://www.minhaconexao.com.br/blog/entenda-o-que-e-a-latencia-e-sua-influencia-na-conexao-com-a-internet/>. Accessed on: 14 Aug. 2021.
4. Forouzan BA. Comunicação de Dados e Redes de Computadores. AMGH Editora, 2009.
5. Medeiros L. Explicando o que é Banda, Taxa de Transferência e Velocidade para Técnicos. SLA Consultorias e Treinamentos, 5 April 2021. Available at: <https://www.youtube.com/watch?v=zxNoNxZJSi8>. Accessed on: 14 Aug. 2021.
6. Ribeiro CHP. Redes de sensores sem fio. Universidade Federal do Rio de Janeiro, Rio de Janeiro, 6 June 2008. Available at: <https://www.gta.ufrj.br/grad/08_1/rssf/CaractersticasdaRede.html>. Accessed on: 14 Aug. 2021.
7. Araújo PD, Márcia L. Estudo comparativo entre redes WIMAX e redes MESH. Available at: https://silo.tips/download/estudo-comparativo-entre-redes-wimax-e-redes-mesh. Accessed on: 14 Aug. 2021.
8. Savoine MM,et al. Proposta de uso de métodos ágeis no gerenciamento e implantação de projeto de redes sem fio. Anais SULCOMP 2017(8).
9. What is LPWAN. Behrtech. Available at: https://behrtech.com/lpwan-technology/. Accessed on: 15 June 2021.
10. Behr A. How new LPWAN standard addresses challenges in connective pumps. Pumps & Systems. Available at:https://www.pumpsandsystems.com/how-new-lpwan-standard-addresses-challenges-connective-pumps. Accessed on: 15 June 2021.
11. Entenda o que é NB-IoT e LTE-M, redes dedicadas a projetos de IoT. Embratel.Available at: https://mundomaistech.com.br/iot/entenda-o-que-e-nb-iot-e-lte-m-redes-dedicadas-a-projetos-de-iot/. Accessed on: 15 June 2021.
12. Sumiyoshi L. Protocolos de IoT: qual a melhor para o seu negócio? Venturus. Available at:https://www.venturus.org.br/protocolos-de-iot-qual-e-o-melhor-para-o-seu-negocio/. Accessed on: 14 Aug. 2021.
13. Bertoleti P. Webinar: Qual LPWAN utilizar: LoRaWAN ou Sigfox? Embarcados tv, 3 July. 2020. Available at: <https://www.youtube.com/watch?v=IOoZ7tXcGpc>. Accessed on: 14 July. 2021.
14. Almeida O. Sigfox X LoRa :Qual a tecnologia ideal para sua aplicação. Connect Five, São Paulo, June, 2020. Available at: https://connectfive.com.br/sigfox-x-lora-qual-a-tecnologia-ideal-para-a-sua-aplicacao/ . Accessed on:17 June 2021.
15. Dellalibera LA. Técnicas de múltiplo acesso para redes LoRaWAN.Trabalho de conclusão de curso-Câmpus experimental de São João da Boa Vista-Universidade Estadual "Júlio de Mesquita Filho", São João da Boa Vista, 2018.
16. Brito I, et al. Openwimesh: um framework para redes mesh sem fio definidas por software. 32th Simpósio Brasileiro de Redes de Computadores e Sistemas Distribuıdos (SBRC) 2014:413-426.
17. Mosquera ED, Gonzalez JAC. Communications system for a soil monitoring network in Valle del Cauca, Colombia, 2015 Workshop on Engineering Applications - International Congress on Engineering (WEA) 2015:1-5.
18. Wireless Connectivity for Massive Scale IoT Deployments. BEHRTECH. Available at: <https://behrtech.com/resources/ebook-wireless-connectivity-for-massive-scale-iot-networking/>. Accessed on: 15 July 2021.
19. Lima GC, Fiorese V, Domingos D, Haiying R. Seminário 5G e IoT na prática, status internacional. Fórum Brasileiro de Internet das Coisas, 29 July 2021. Available at: <https://www.youtube.com/watch?v=BUCd-qAk6n8&t=3s>. Accessed on: 29 July 2021.
20. What is CBRS?-LTE in 3.5GHz Shared Spectrum and What it Means for IoT. Leverege, 9 June 2017. Available at: <https://www.leverege.com/blogpost/what-is-cbrs-lte-3-5-ghz>. Accessed on: 13 Aug. 2021.
21. Yavuz M. Private mobile networks as a foundation for smart industry.
22. Mun K. CBRS: New shared spectrum enables flexible indoor and outdoor mobile solutions and new business models. White Paper 2017(Mar).

Technological Prospecting for Enhanced Oil Recovery Methods in Onshore Scenarios for the Brazilian Field Application – A Literature Review

Thaylanne Kadman Costa Duarte[1*], Gabriel Malgaresi[1], Fernando Luiz Pellegrini Pessoa[1]
[1]SENAI CIMATEC University Center; Salvador, Bahia Brazil

Enhanced oil recovery (EOR) methods are adopted when the reservoir is not auto-sufficient energetically or even after secondary oil recovery and the reservoir is not producing satisfactorily. This article aims to perform a literature review of EOR methods, starting from the applied techniques worldwide in onshore fields and proposing implementation in Brazilian onshore scenarios. This initial work studied polymer flooding combustion in situ and cyclic steam in onshore fields. The most promising studied method was combustion in situ due to its higher recovery factor. However, further studies are necessary to understand better more cases of EOR methods applied in onshore scenarios.
Keywords: Onshore. EOR. Polymer Flooding. *In situ* Combustion. Cyclic Steam.

Introduction

Oil use has been presented in the history of human life since antiquity. However, the Nineteenth century became an energy source on a large scale nowadays due to its versatility and wide usability. However, this energy source is not renewable, and after continuous production, oil reservoirs mature, and consequently, its production declines and becomes not economically viable. Therefore, it is necessary to use non-conventional oil recovery methods [1].

Enhanced oil recovery (EOR) methods are implemented when reservoirs cannot produce satisfactory using their energy or after a secondary recovery method. Among these EOR methods, thermal methods provide heat to the reservoir, raising the temperature to reduce the oil viscosity and allowing higher mobility. As examples of EOR thermal methods, we can cite cyclic steam injection and *in situ* combustion [2-4].

Another way to improve the oil recovery factor is by injecting chemical agents, such as polymers and surfactants. This method usually changes the property of the injected fluid to increase its viscosity, reducing the injected fluid's mobility and consequently generating a better oil sweep. Another approach of this method changes the wettability alteration of the reservoir or interfacial tension between oil/water by chemical adsorption in the surface reservoir and oil/water interface, respectively [1,5].

In this context, this article aims to perform a literature review of advanced oil recovery methods used worldwide to identify the most promising method for later implementation in Brazilian onshore fields. In this initial work, we studied and understood EOR methods such as polymer flooding, in-situ combustion, and cyclic steam injection for further possible application in Brazilian onshore scenarios.

Materials and Methods

This paper provides a literature review of the most used EOR in onshore scenarios. We conducted the research from April to August 2021. First, we investigated the main methods of enhanced oil recovery to increase the oil recovery factor in onshore fields worldwide. The selected keywords to find the papers, articles, and all material used in this work were: Enhanced Oil Recovery; EOR; and Onshore. The combination of these three elements provides the following search string: [(Enhanced Oil Recovery OR EOR) AND Onshore")]. The inclusion criteria used to develop this literature

Received on 25 June 2022; revised 24 August 2022.
Address for correspondence: Thaylanne Kadman Costa Duarte. Av. Orlando Gomes, 1845 - Piatã, Salvador - BA-Brazil. Zipcode: 41650-010. E-mail: thay.crf@gmail.com.
DOI 10.34178/jbth.v5i3.226.

J Bioeng. Tech. Health 2022;5(3):190-195

review were: (i) Only articles in Portuguese or English language were mapped; (ii) EOR methods worldwide were considered; (iii) Only articles from 2011 to 2021 were considered. The exclusion criteria were: (i) EOR methods applied on offshore fields; (ii) articles with titles and abstracts not compatible with the objective of this research. The search base of this work was: ScienceDirect, OnePetro, COBEQ (Congresso Brasileiro de Engenharia Química), and Scholar google in general. The first base provided 1,110 articles, then 1,061, 1, and 6,740 at the final. The sum of the three platforms results in 7912 works. We chose three papers based on their application for this initial study.

After all this stage, we herein evaluate and understand each EOR method already used in different countries to use the promising method in Brazil's onshore scenarios. We critically analyze each case reported in the literature (Figure 1).

Figure 1. Description of literature research methodology.

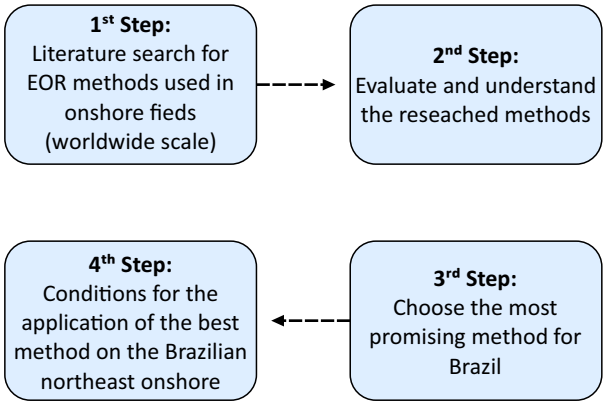

Results and Discussion

This section presents a brief literature review of three EOR methods applied in different countries in onshore fields. We used only journals and cases applied in the field in this systematic mapping.

Polymer Flooding

Polymer injection is an advanced oil recovery method used worldwide for several decades. The injected polymers increase the viscosity of the injected water, improving the oil-water mobility ratio. In addition, it brings the viscosity closer to the oil to achieve a unity mobility rate, enabling a more significant oil recovery due to the efficiency of the vertical sweep and the larger water injection area [6,7]. Prasad and colleagues (2014) performed a study in Mangala (India), which contains sweet crude oil, where its density ranges from 20 to 28º. API and implementation of hot water injection from the beginning of production, aiming to keep the pressure of the reservoir. After evaluations, a 60% water cut and simulation studies verified that Mangala field was a candidate for a polymer injection such as the EOR method, making it possible to conduct a pilot project. This trial consisted of 8 wells, four injectors, one producer, and three for observation, this last type with a 100m x 100m area. The pilot project results showed that the addition of the polymer matched the expectations and was promising, with an increase in oil recovery and a decrease in the water cut (Figure 2).

After the positive pilot project results, the authors intend to inject polymer throughout the field. The results obtained from the simulation (Figure 3) demonstrated a higher oil sweep in polymer injection compared to hot water injection. It occurs due to the rising water viscosity, which becomes closer to the oil viscosity, thus improving the ratio of oil-water mobility.

In situ Combustion (ISC)

In heavy oil reservoirs, an appropriate oil recovery method is in-situ combustion. In this process, the oxygen in the injected air reacts with the hydrocarbons in the reservoir, releasing heat in the combustion zone. Then, the heat released vaporizes the lighter fraction of the oil, forming a steam zone that heats it, decreasing its viscosity. This process allows it to move towards the producing well, forming a zone of heated oil, and

Figure 2. Pilot project performance.

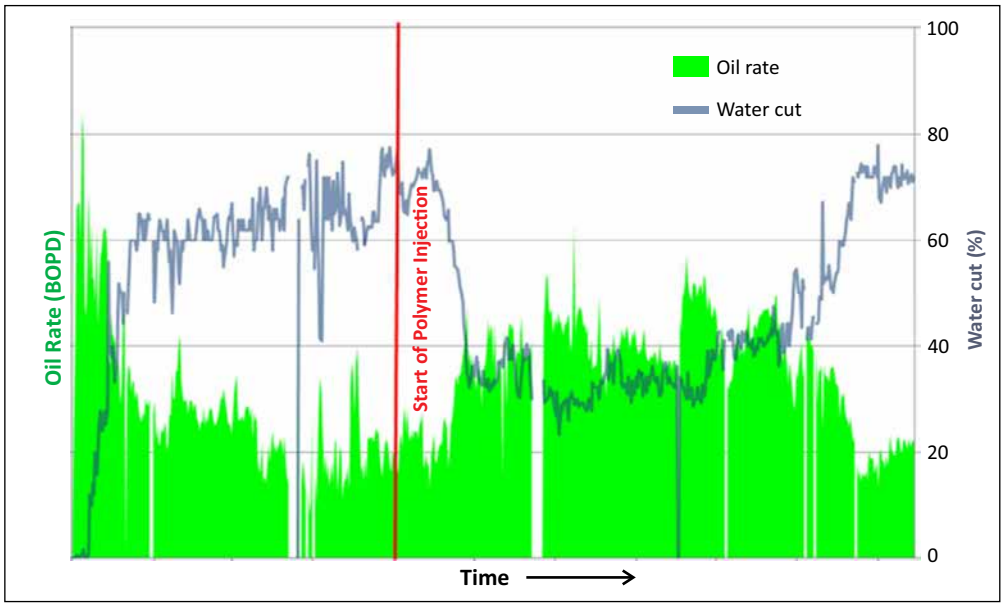

Source: Prasad and colleagues (2014) [5].

Figure 3. Improved areal sweep in one of the top layers in Mangala after ten years of polymer flooding.

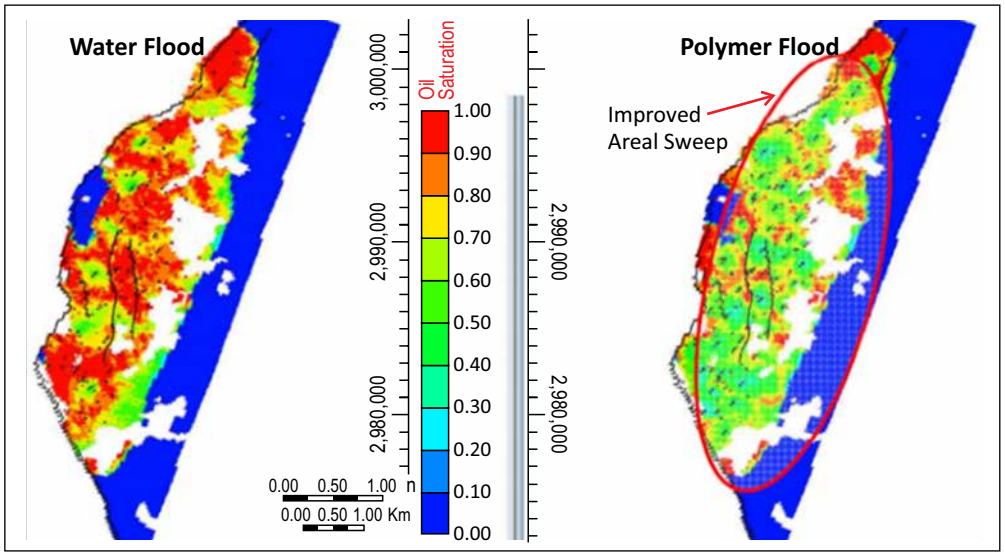

Source: Prasad and colleagues (2014) [5].

the water in the reservoir is also heated. Gases from the combustion reaction, oil vaporization, and water steam are also sought with the oil [2,8]. Using the STARS simulator ("Steam, Thermal, and Advanced Processes Reservoir Simulator") from the CMG group ("Computer Modelling Group"), Rocha and colleagues (2014) conducted a study of an *in situ* combustion application in a homogeneous reservoir with similar characteristics of Brazilian's northeastern. This work aims to analyze the recovery of oil and the percentage of oxygen consumed, varying the air injection flows, the completion of the injector well, and oxygen concentration. The process begins with air injection in the reservoir to ignite part of the existing oil, producing heat. In this technique, the air is injected through a vertical well while a horizontal well extracts the oil, called the Toe-To-Heel Air Injection (THAI) (Figure 4).

Figure 4. Schematic of the THAI™ and CAPRI™ processes showing the vertical air injector, combustion zone, coke zone, mobilized oil zone, and the catalyst-lined horizontal production well.

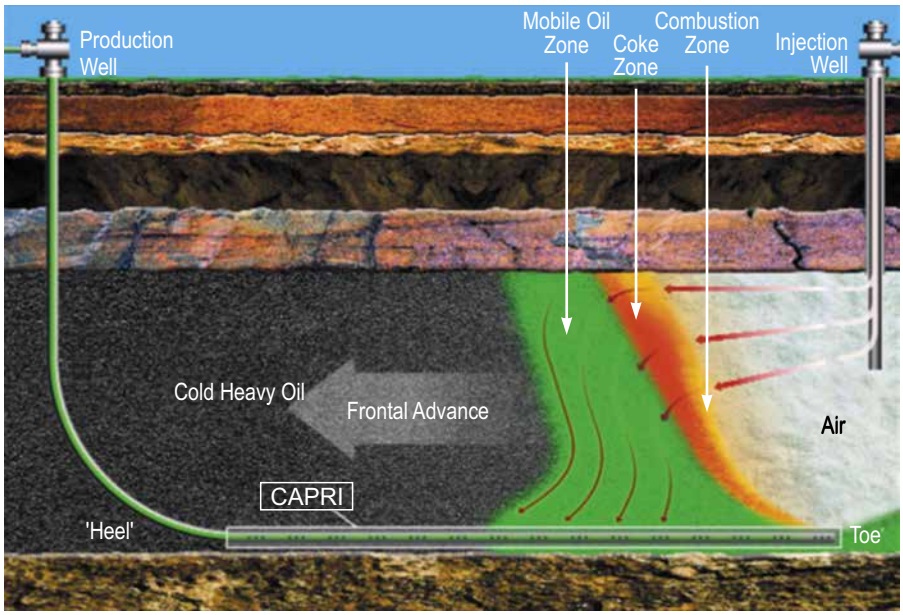

For better analysis of the influence of each parameter, the authors created a table containing the 18 simulated cases, considering the variation of injection flow, well completion, and oxygen concentration. We organized the cases in a decreasing way of the oil recovery factor (%FR) found in 20 years of production (Figure 5).

Among the simulated cases, the best result achieved was when oxygen concentration and air injection flow at a minimum level were 21% and 15,000 m³ std/day, respectively. We plotted a Pareto diagram to verify the influence of each of the variables (Figure 6). We checked it when the oxygen concentration had the most significant effect on the oil recovery factor (%Fr) and related to the excellent completion configurations, and the lower completion demonstrated the best results.

Cyclic Steam

Cyclic steam injection is a process that performs a good stimulation that involves the transfer of heat to the reservoir near the wellbore by a periodical injection of steam [9,10]. Beallessio and colleagues (2021) reported using cyclic steam as an advanced recovery method (EOR) in Kazakhstan. By possessing heavy oil in shallow depths, the Kenkiyak field was an excellent candidate for this EOR method, and since 1975 wet steam (saturated) has been injected into the well, obtaining good results. In 2006, a pilot project using an overheated cyclic steam injection proved promising. This method was able to increase 61.9% the oil recovery rate.

This advantage is due to the temperature of overheated steam, which is higher than the water boiling temperature. This fact allows it to travel through the surface infrastructure, decreasing until the well and not condensing, despite the heat loss, reducing the viscosity of the oil and increasing recovery. However, this process has a more efficient sweep concerning saturated steam, and more combustible gas is needed to generate overheated steam compared to the expenditure on saturated steam, increasing the financial cost. Table 1 compiles the methods found, referring to each country that has used the aforementioned methods, the size of the field, and the additional recovery factor found.

Figure 5. Recovery factor for simulated cases.

	O_2 Consumption	Injection Flow	Injection Completion	RF(%) 5 years	RF(%) 10 years	RF(%) 15 years	RF(%) 20 years
Case 13	21%	15,000	Bottom	2.38	17.00	58.12	63.09
Case 1	21%	15,000	Top	2.09	5.68	59.00	63.00
Case 7	21%	15,000	Middle	2.22	10.27	58.00	62.89
Case 14	21%	20,000	Bottom	2.38	43.46	59.00	59.77
Case 2	21%	20,000	Top	2.05	43.10	57.81	59.12
Case 8	21%	20,000	Middle	2.22	42.92	58.00	59.00
Case 15	21%	25,000	Bottom	6.27	52.59	56.77	57.16
Case 9	21%	25,000	Middle	5.55	52.24	55.73	56.37
Case 3	21%	25,000	Top	4.50	52.64	55.00	56.01
Case 16	50%	15,000	Buttom	20.06	52.86	53.73	54.44
Case 10	50%	15,000	Middle	19.60	51.73	52.62	53.83
Case 4	50%	15,000	Top	19.06	49.87	51.14	52.90
Case 17	50%	20,000	Buttom	33.35	50.47	51.87	52.17
Case 18	50%	25,000	Buttom	41.12	49.28	51.07	51.31
Case 11	50%	20,000	Middle	33.12	48.64	49.95	50.84
Case 5	50%	20,000	Top	32.82	46.65	48.17	49.56
Case 12	50%	25,000	Middle	40.58	47.32	48.98	49.48
Case 6	50%	25,000	Top	39.43	45.49	46.94	47.97

Source: Rocha and colleagues (2014) [3].

Figure 6. Pareto diagram of operational variables.

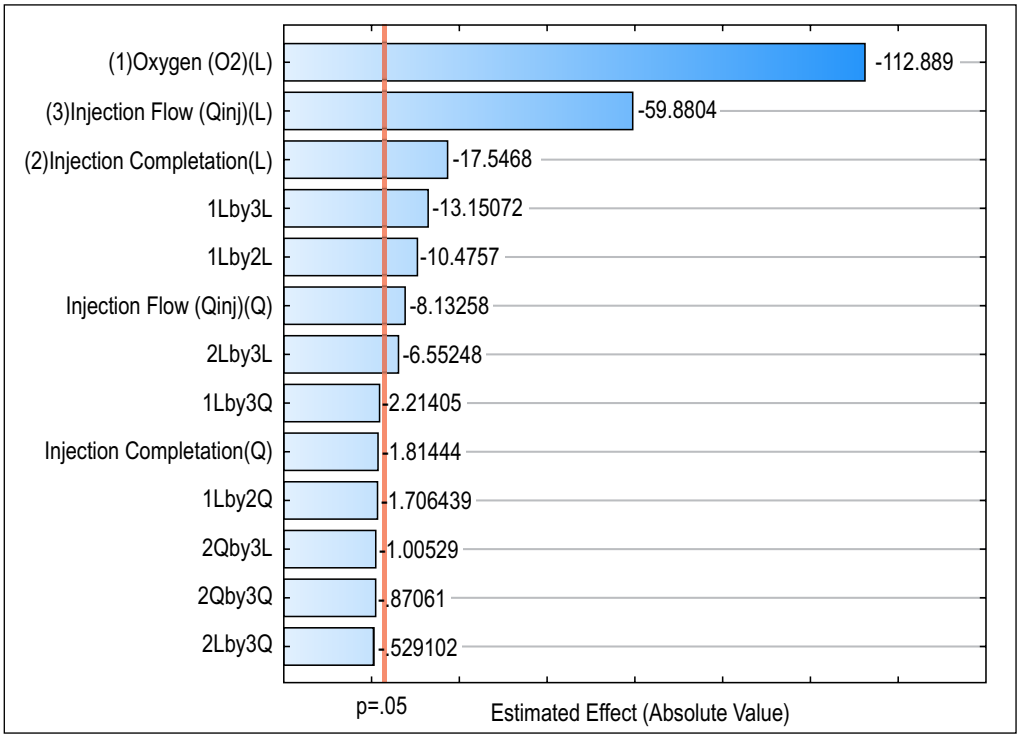

Purpose Function: oil recovered in 20 years.
Source: Rocha and colleagues (2014) [3].

Table 1. The method used in each country.

Countries	EOR Method	Field Size/Oil in Place	Additional Recovery Factor
India	Polymer Flooding	100 m x 100 m	~ 55%
Kazakhstan	Cyclic Steam	-	61.9%
Brazil	*In situ* Combustion	100 m x 100 m	63.9%

Conclusion

This initial study found in-situ combustion to be the most promising EOR method for onshore scenarios due to its higher oil recovery factor. However, to better understand the research topic and identify the best EOR technique for Brazilian onshore fields, it is necessary to study more articles and cases beyond the methods already mentioned. In parallel, we also intend to provide an economic feasibility study to evaluate the implementation of these methods in the Brazilian northeastern onshore fields.

Acknowledgments

The authors thank PRH 27.1, ANP/FINEP, Centro de Competências de Soluções Integradas Onshore, and SENAI/CIMATEC for the financial support and research incentives.

References

1. Marques LS, et al. Prospecção tecnológica sobre recuperação avançada de petróleo (EOR) com associações de fluídos de naturezas químicas diferentes. Cadernos de Prospecção 2014;7(2):247.
2. Araújo EA. Estudo do processo de combustão *in situ* usando poços horizontais como produtores de óleo (Toe-to-Hell Air Injection). 2012. Dissertação de Mestrado. Universidade Federal do Rio Grande do Norte.
3. Rocha ML, Araújo EA, Barillas JLM.Estudo da combustão *in situ* em reservatórios com características do Nordeste brasileiro. In: XX Congresso Brasileiro de Engenharia Química, Florianópolis, SC. 2014.
4. Bealessio BA, et al. A review of enhanced oil recovery (EOR) methods applied in Kazakhstan. Petroleum 2021;(7)1:1-9.
5. Prasad D, et al. Pilot to full-field polymer application in one of the largest onshore field in India. In: SPE Improved Oil Recovery Symposium. OnePetro 2014.
6. Silva IG, et al. Polymer flooding: A sustainable enhanced oil recovery in the current scenario. In: Latin American & Caribbean Petroleum Engineering Conference. OnePetro 2007.
7. Firozjaii AM, Saghafi HR. Review on chemical enhanced oil recovery using polymer flooding: Fundamentals, experimental and numerical simulation. Petroleum 2020;(6)2:115-122.
8. Kendall Rob. Using timelapse seismic to monitor the THAI™ heavy oil production process. In: SEG Technical Program Expanded Abstracts 2009. Society of Exploration Geophysicists 2009:3954-3958.
9. Alikhlalov K, Dindoruk B. Conversion of cyclic steam injection to continous steam injection. In: SPE Annual Technical Conference and Exhibition. OnePetro 2011.
10. Muñoz M.Current overview of cyclic steam injection process. Journal of Petroleum Science Research 2013.

Technologies for Air Conditioning Powered by Alternative Energy Sources: A Brief Review

Ana Caroline Neves dos Santos[1*], Alex Álisson Bandeira Santos[1]
[1]SENAI CIMATEC University Center; Salvador, Bahia Brazil

Air conditioning systems promote human comfort, representing an energy consumption of up to 30% in a building. Although electric chillers are still widely used for thermal comfort, absorption chillers are a promising alternative for air conditioning using renewable energy sources (solar energy, natural gas, waste heat, geothermal, and biomass). The search for efficient, economical, and ecological solutions becomes evident regarding these considerations. This article proposes a brief bibliographical review of chillers powered by alternative energy sources to electricity. Awareness of the application of alternative energy sources in these systems contributes to sustainable practice and energy matrix diversification.
Keywords: Absorption Chiller. Air Conditioning. Alternative Energy Sources.

Introduction

The balance between environmental conservation and sustainable economic development has been a recurring societal issue. In order to preserve the environment at the expense of exacerbated consumption, environmental policies are becoming increasingly strict regarding primary energy consumption [1].

Because of the global energy scenario, the need to expand the energy matrix and promote sustainable development is evident; seeking alternative and renewable energy sources, as well as the use and better application of these, have become required in this century [2]. When analyzing the energy matrix in its global context, it is clear that only 13.8% is derived from renewable sources, namely: biomass (9.3%), hydraulics (2.5%), and others - solar, wind, and geothermal (2.0%) [3]. Compared to the Brazilian scenario, 46.2% of the energy matrix comes from a renewable source. However, when analyzing the renewable part of the Brazilian energy matrix, only 7% derives from solar, wind, and geothermal energy, and the other 39.2% comes from hydraulics (12.4%), sugarcane derivatives (18%) and firewood and charcoal (8%) [4].

Although the Brazilian matrix comes considerably from renewable sources, the socio-environmental impacts of some of these sources are considerable when compared to other energy sources [5].

The correlation between the evolution of energy demand and economic growth measured by GDP has been recurrent, and the increase in energy consumption can be attributed to air conditioning systems [6]. The demand for the expansion in using air conditioning and refrigeration systems occurred due to population growth, global warming, the increase in the social standard of living, and architectural characteristics, among others [7,8]. In addition, air conditioning systems consume around 30% of an enterprise's energy demand in different sectors (homes, schools, canteens, public offices, hospitals, and markets) [9].

Materials and Methods

This article presents a literature review on alternative energy sources used in chillers for air conditioning. First, we did quantitative research to find alternative sources for HVAC chillers. Then, we searched for articles from the last six years related to the topic (quantitative and qualitative analysis) and excluded duplicates. Figure 1 shows the described method.

Received on 28 June 2022; revised 20 August 2022.
Address for correspondence: Ana Caroline Neves dos Santos. Rua dos Pintassilgos, 202, Imbuí, Salvador-BA. CEP: 41720-030. Email: carolneves1@gmail.com.DOI 10.34178/jbth.v5i3.227.

J Bioeng. Tech. Health 2022;5(3):196-201

Figure 1. Literature review method.

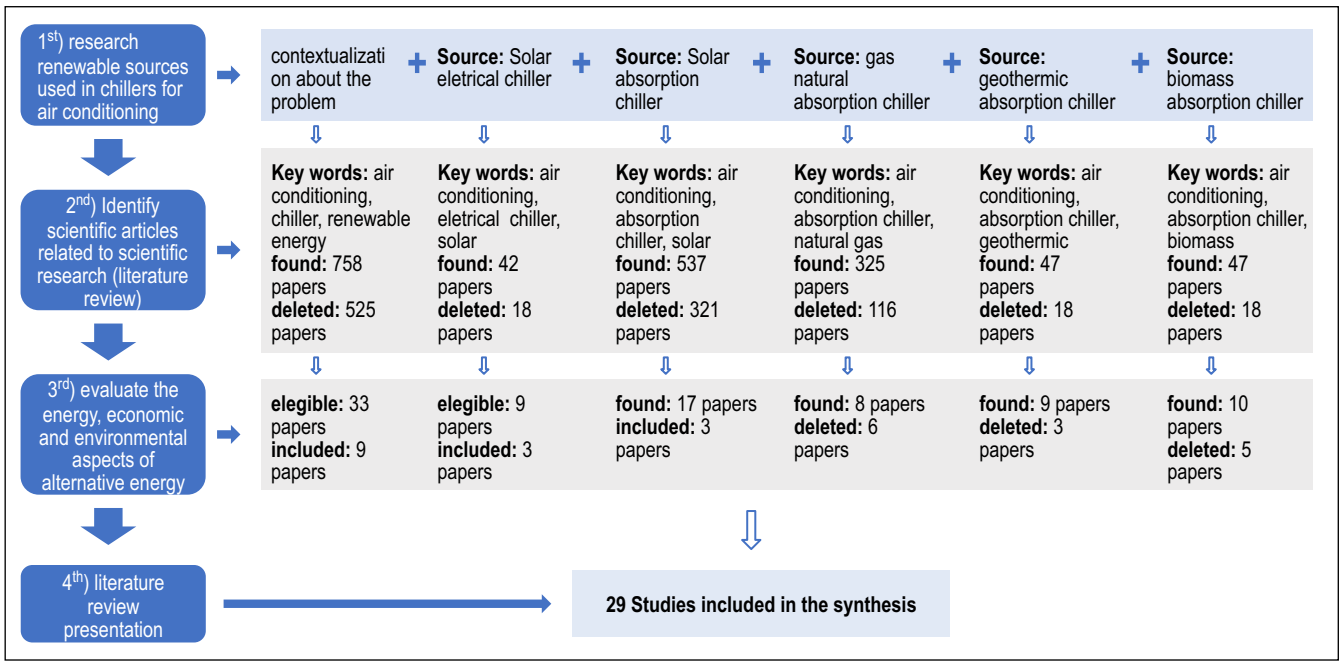

Source: By authors.

Results and Discussion (Figure 2 and Box 1)

Based on thermodynamic principles, the equipment used in air conditioning systems for cold production (chillers) is mainly powered by electricity. The literature estimates that this equipment contributes about 10% to the greenhouse effect and consumes 15% of the energy distributed globally. Therefore, chillers are responsible for the highest energy consumption in air conditioning installations. Some chillers are powered by electrical energy (considered noble energy), having the thermodynamic cycle of vapor compression (CCV) as the basic principle of the thermal machine. There are also absorption chillers based on the thermodynamic absorption cycle (CA). This equipment is promising for diversifying the energy matrix using renewable energy sources [10].

The absorption technology is advancing and gaining more expansive implementation for cooling. However, mechanical vapor-compression-air-conditioning systems are still widely used in many commercial, residential, and industrial installations. It occurs due to the low input energy requirement of the absorption chillers, which are ecological and powered by sources of solar energy, waste heat, geothermal, and biomass [9-11]. The use of solar energy as a primary energy source is in rapid development and implementation due to its potential to diversify the energy matrix and because the cooling loads coincide with the greater availability of solar energy offered [11]. Usually, the low heat provided by the solar collector, especially the photovoltaic (PV) panels, does not meet the temperature required to activate chillers, leading to unsatisfactory system performance. Therefore, it is necessary to use an auxiliary energy system (SAE) to supply the demand [12]. CCV chillers that use PV energy as a primary source (and electrical energy as SAE) can play a positive role in sustainability. Due to their simple installation and reliability, PV became applicable, efficient, and economically viable. When associated with thermal collectors (T) - PV/T systems - they offer new fields of application offering economic and energy benefits [13,14]. The single-effect air-cooled lithium-bromide-water absorption chiller (LiBr-H_2O) presents advantages in residential applications and

Figure 2. Alternative energy sources in chillers.

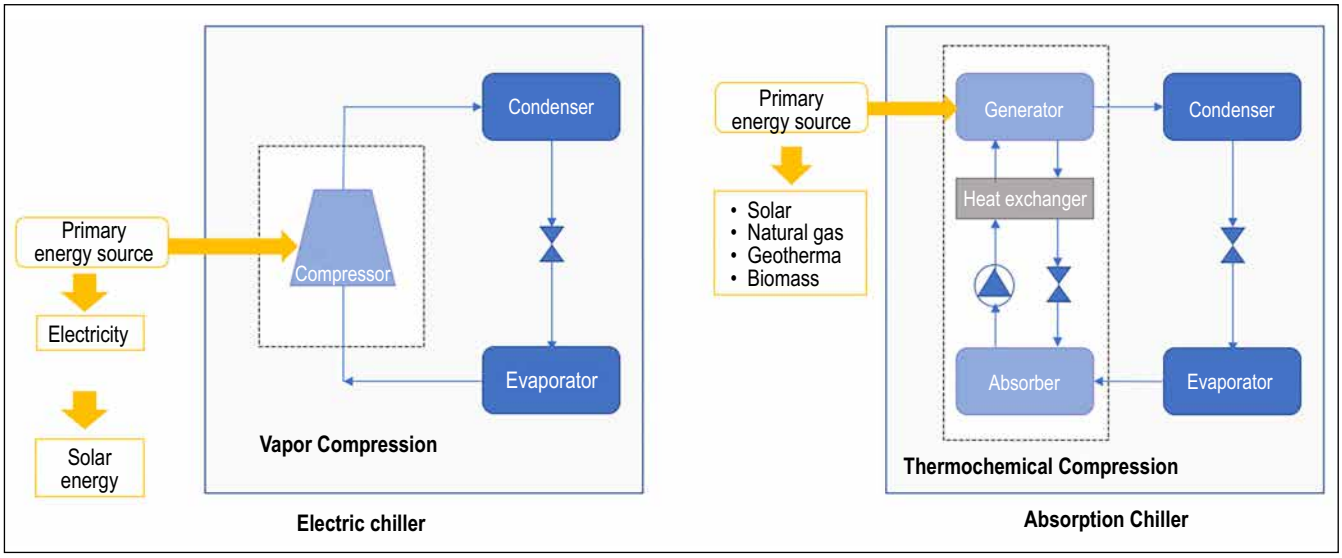

Source: By authors.

has shown to be promising in reducing electrical consumption [15]. Combined with natural gas (SAE), they present satisfactory energy performance [12]. Furthermore, infrastructures that use essentially natural gas absorption chillers can be easily adapted to work with solar energy [11]. Absorption chillers are a promising alternative, exhibiting considerable energy-saving benefits, potential economic viability, and environmentally friendly features [16]. Given the search for alternative energy sources and considering that there are polluting fuels in the atmosphere, such as coal, heavy oil, and tar, natural gas presents itself favorably [7]. When comparing natural gas with other biofuels, there is less CO_2 emission. Furthermore, natural gas is preferred by stakeholders and politicians, as geopolitics often plays an essential role in choosing the appropriate energy source [17]. Natural gas as a primary energy source for the absorption chiller is a promising solution. It presents valid results with high efficiency and an excellent financial return (simple payback of 3.4 years) [18]. When associated with thermal waste as a source of secondary energy allows the reduction of the consumption rate of natural gas and reduces the annual operating cost. This solution can be crucial in energy efficiency and reducing thermal and environmental pollution [19]. Geothermal energy has diverse industrial and domestic applications, including a cold promotion with absorption chillers. Its process consists of providing earth/ground heat for heating and cooling [20]. Geothermal energy is a resource that provides an economic gain, as it is verified an increase in energy efficiency in refrigeration systems and energy generation with absorption chillers. However, it cannot be used efficiently for electricity generation [21]. On the other hand, technologies that use geothermal energy in air conditioning systems have a good performance and can be very competitive when well implemented compared to conventional technologies [22]. Biomass is one of the renewable energy sources with the potential to diversify the energy matrix and promote industrial symbiosis. Its main product – synthesis gas – can be used as fuel in several sectors, including trigeneration. The application of synthesis gas has high energy and environmental value. However, they are not widely applied due to their high complexity and high initial investment [23]. In addition to synthesis gas, biogas, also derived from biomass, can be used as fuel to reduce total greenhouse gas emissions [24]. Although it does not present

significant efficiency gains compared to natural gas, biomass may be a promising alternative in the future because it has impressive environmental advantages and has not reached technological maturity [25]. Pantaleo and colleagues (2017) [26] proposed a mixture of fuel, 50% natural gas, and 50% biomass in a mixed gas microturbine to overcome the barriers to energy efficiency, economic viability, and good profitability. In addition to energy efficiency results, environmental impacts are reduced when biomass is used in trigeneration concerning energy production [27].

Conclusion

We presented the refrigeration systems for air conditioning powered by alternative energy sources as alternatives to market solutions that use electricity as the primary energy for this equipment. The most significant appeal of the application of these technologies is the diversification of the energy matrix and sustainable practice. Despite the diversity of alternative energy sources, the absorption chiller still needs to overcome a market barrier to the detriment of compaction technology.

Box 1. Comparative alternative sources in chillers by literature.

	Energy efficiency	**Economic viability**	**Environmental impact**
Electric chiller - Solar energy	They are efficient, when the PVT system is used, its efficiency is maximized [14]	The economy depends on each country's energy prices and energy policy [18]	Even being renewable, electricity as SAE, has a socio-environmental impact [5]
Absorption Chiller - Solar Energy	When associated with natural gas, they show satisfactory performance [15]	They may have payback between 4 and 5 years [28]	Significantly reduces CO_2 emissions per year [15]
Absorption Chiller - Natural Gas	They are efficient and when combined with thermal waste they are promissing [28, 19]	Feasilble, however, government incentives directly influence [29]	The association with thermal waste provides a reduction in thermal and environmental pollution [19]
Absorption Chiller - Geothermal	Efficient, especially when used for trigeneration [21]	It may be feasible when there is no incentive to other sources [20]	Reduced environmental impacts [22]
Absorption Chiller - Biomass	Compared to natural gas, biomass has not shown significant energy efficiency gains [24]	In mixtures (50% natural gas and 50% biomass) it is profitable both trigeneration and cogeneration [27]	They are reduced, especially when used for trigeneration [27]

Source: By authors.

One way to enable superior technology in economic incentive technologies is in the commercialization of solar collectors, government incentives for the use of natural gas and solar energy, and more significant technological investment to make the use of geothermal energy and biomass feasible. Even with the challenges faced, the community must be aware of the various alternatives for air conditioning so that there are technological advances without compromising the environment.

Acknowledgments

The authors thank FAPESB and SENAI/CIMATEC for their support and encouragement of the research.

References

1. Petela K, Manfrida G, Szlek A. Advantages of variable driving temperature in solar absorption chiller. Renewable Energy 2017;114:716-724.
2. Silva DH. Protocolos de Montreal e Kyoto: pontos em comum e diferenças fundamentais. Revista Brasileira de Política Internacional 2009;52(2):155-172.
3. International Energy Agency. World energy balances database (2018). 2020. Disponível em: https://www.iea.org/data-and-statistics?country=WORLD&fuel=Energy%20consumption&indicator=TFCbySource. Acesso em: 11 fev. 2021.
4. Empresa de Pesquisa Energética (org.). Balanço Energético Nacional 2020: Ano base 2019. Empresa de Pesquisa Energética, Rio de Janeiro. 2020. 292 p. Disponível em: https://www.epe.gov.br/sites-pt/publicacoes-dados-abertos/publicacoes/PublicacoesArquivos/publicacao-479/topico-528/BEN2020_sp.pdf. Acesso em: 11 fev. 2021.
5. Silveira PG. Energia e mudanças climáticas: impactos socioambientais das hidrelétricas e diversificação da matriz energética brasileira. Opinión Jurídica 2018;17(33):123-148.
6. Mura PG, Innamorati R. Design of a new Ssstem of high-power efficiency conditioning cogeneration energy for a building of the University of Cagliari with fossil fuel plants. Energy Procedia 2015;78:1111-1116.
7. Mehmood S, et al. Energetic, economic and environmental (3E) assessment and design of solar-powered HVAC systems in Pakistan. Energies 2020;13(17):4333-4363.
8. Allouhi A, et al. Solar driven cooling systems: Updated review. Renewable and Sustainable Energy Reviews 2015;44:159-181.
9. Mansouri R, et al. Modelling and testing the performance of a 7omercial ammonia/water absorption chiller using Aspen-Plus platform. Energy 2015;93:2374-2383.
10. She X, Cong L, Nie B, Leng G, Peng H, Chen Y, Zhang X, Wen T, Yang H, Luo Y. Energy-efficient and economic technologies for air conditioning with vapor compression refrigeration: a comprehensive review. Applied Energy 2018;232:157-186.
11. Shirazi A, et al. A comprehensive, multi-objective optimization of solar-powered absorption chiller systems for air-conditioning applications. Energy Conversion And Management 2017;132:281-306.
12. Li ZL, et al. Comprehensive evaluation of low-grade solar trigeneration system by photovoltaic-thermal collectors. Energy Conversion and Management 2020;215(112895).
13. Al-Falahi A, et al. A new design of an integrated solar absorption cooling system driven by an evacuated tube collector: A case study for Baghdad, Iraq. Applied Sciences 2020;10(10):3622-3645.
14. Mao Y, Wu J, Zhang W. An effective operation strategy for CCHP system integrated with photovoltaic/thermal panels and thermal energy storage. Energies 2020;13(23):6418.
15. Alhami MI, et al. Energy analysis for the solar thermal cooling system in Universitas Indonesia. International Journal of Air-Conditioning and Refrigeration 2019;27(3).
16. Sarbu I, et al. General review of solar-powered closed sorption refrigeration systems. Energy Conversion and Management 2015;105:403-422.
17. Balitskiy S, et al. Energy efficiency and natural gas consumption in the comercial of economic development in the European Union. Renewable And Sustainable Energy Reviews 2016;55:156-168.
18. Alcântara SCS, et al. Natural gas based trigeneration system proposal to an ice cream factory: an energetic and economic assessment. Energy Conversion and Management 2019;197:111860.
19. Semmari H, et al. Flare gas waste heat recovery: Assessment of organic rankine cycle for electricity production and possible coupling with absorption chiller. Energies 2020;13(9):2265.
20. Zare V. A comparative thermodynamic analysis of two tri-generation systems utilizing low-grade geothermal energy. Energy Conversion and Management 2016;118:264-274.
21. Kececiler A, Acar H, Dogean A. Thermodynamic analysis of the absorption refrigeration system with geothermal energy: an experimental study. Energy Conversion & Management 2000;41:37-48.
22. Thornton JW, McDowell TP, Hughes P. J. Comparison of practical vertical ground heat exchanger sizing methods to a Fort Polk data/model benchmark. American Society of Heating, Refrigerating, and Air-Conditioning Engineers (ASHRAE) 1997;103.

23. Segurado R, Pereira S, Correia D, Costa M. Techno-economic analysis of a trigeneration system based on biomass gasification. Renewable And Sustainable Energy Reviews 2019;103:501-514.
24. Jabari F, et al. Design and performance investigation of a biogas fueled combined cooling and power generation system. Energy Conversion and Management 2018;169:371-382.
25. Freire RMMS, Santos AAB, Almeida AGS. Thermoeconomic evaluation of three proposals for the energy cogeneration unit powered by natural gas, biogas, or syngas. Journal of The Brazilian Society of Mechanical Sciences and Engineering 2020;42(8):440.
26. Pantaleo AM, et al. Energy performance and thermo-economic assessment of a microturbine-based dual-fuel gas-biomass trigeneration system. Energy Procedia 2017;105:764-772.
27. Gholamian E, Zare V, Mousavi SM. Integration of biomass gasification with a solid oxide fuel cell in a combined cooling, heating and power system: A thermodynamic and environmental analysis. International Journal of Hydrogen Energy 2016;41(44):20396-20406.
28. Ibrahim NI, Al-Sulaiman FA, Ani FS. A detailed parametric study of a solar driven double-effect absorption chiller under various solar radiation data. Journal of Cleaner Production 2020;251:119750.
29. Linjawi MT, Talal Q, Al-Sulaiman FA. Evaluation of solar thermal driven cooling system in office buildings in Saudi Arabia. E3S Web of Conferences 2017;23:5001.

2D Image Object Detection Aided by Generative Adversarial Networks: A Literature Review

Caio Vinicius Bertolini[1*], Roberto Monteiro[1]
[1]SENAI CIMATEC University Center; Salvador, Bahia Brazil

Object Detection (OD) is one of the most critical tasks in 2D image processing. The researchers proposed multiple math models and frameworks based on Deep Convolutional Networks, such as R-CNN, SSD, and YOLO are the most common. Generative Adversarial Nets (GAN) represent a prominent field of study in machine learning, and it has been applied to many tasks with exciting results. This work aims to assess the potential of GANs applied to OD tasks and the proposed frameworks as a field of study. The methodology used was a systemic review of 14 papers. The conclusion shows that although OD and GANs are popular themes, there are not many developments in the intersection of both subjects. Therefore, OD with GAN-applied tasks is an excellent field to explore in future works.
Keywords: Generative Adversarial Nets. Object Detection. Deep Learning.

Introduction

Digital Images captured by cameras are very common today as the number of such devices spiked over the last years. The captured images are no longer used only for entertainment or as an art form. Instead, they have become an essential data source that can be analyzed. In such a way that cameras are one of the most common sensors and are present in smartphones, vehicles, smart house devices, city security systems, and many others. Many aspects of an image can be analyzed, and one of the most common problems to solve is object detection in 2D images. The object detection task combines two other assignments: object classification, which identifies the type of object detected, and object localization, which identifies the object's location in the image.

The object detection problem has been gaining significant attention from the academic community and increasing momentum in publications over the last few years. Viola-Jones Detectors, HOG Detector, and Deformable Part-based Models (DPM) are some object detection frameworks. However, Deep Learning techniques, and the ones based on Convolutional Neural Networks (CNN), represented a big leap in accuracy and are the most used today [1].

Today, there are two main categories of object detectors:

1. Two-Stage Object Detectors, which separate the detection tasks of classification and localization to be held by different parts of the network
2. Single Stage Object Detectors, which do the classification and localization tasks all at once.

Two-Stage Object Detectors

The Regions with CNN (R-CNN) [2] framework consists of an initial selective search that generates region proposals by close-by pixels similarities. Then each proposed region is fed into a CNN for feature extraction. The output is used as input of bound-box regression and classification Support Vector Machine (SVM) to define if there is an object in the proposed region and what class it is. The framework presented higher Average Precision (AP) than existing methods for multiple classes [2] but with a high computational cost as it performs the redundant computation in the overlapping features of the many proposed regions. [1] Fast R-CNN [3] and SPPNet [4] apply the CNN only once in the entire image and not many times in the multiple proposed regions as per R-CNN. While

Received on 12 June 2022; revised 20 August 2022.
Address for correspondence: Caio Vinicius Bertolini. R. Dr. Barreto, 203 - apto 504V - Lauro de Freitas - BA, Brazil | CEP: 42701-310. DOI 10.34178/jbth.v5i3.228.

J Bioeng. Tech. Health 2022;5(3):202-207.

Fast R-CNN uses a Region of Interest (RoI) pooling with Fully Connected (FC) layers for classification and bounding box regression [3], SPPNet uses a Spatial Pyramid Pooling (SPP) to define the regions, which also allows for different image input sizes [4].

Faster R-CNN [5] presents inference results 34 times faster than Fast R-CNN. It happens due to the introduction of Anchor boxes and a specific Fully Convolutional Network (FCN) to generate the Region of Interest (RoI), the Region Proposed Network (RPN). The RPN uses the Anchor boxes as inputs and Intersection over Union (IoU) metrics to define the RoI bounding boxes. After that, it uses the Non-Maximum Suppression (NMS) technique to define a final bounding box. The RPN is trained together with the rest of the model, and the region outputs then pass through the RoI pooling and the FC layers for classification and bounding box regression, similarly to the Fast R-CNN [5].

Single-Stage Object Detectors

You Only Look Once (YOLO) [6] method process the entire image by a CNN-based model with multiple Anchor Boxes that simultaneously predict the class and location of the bounding boxes. Then, the bounding boxes within a pre-defined threshold are subjected to NMS to define the final bounding box for each object.

Single Shot Multibox Detector (SSD) [7] also uses multi Anchor boxes. In SSD, after the image passes through the feature extractor, it then goes by Multi-scale feature layers, which decrease in size at each step and allow predictions of detections at multiple scales at once. This ability to detect in multi-resolution and scales is the main contribution of SSD and presents an advantage in average precision compared to YOLO. The last step of SSD is NMS which eliminates the overlapping bounding boxes [1,7].

Generative Adversarial Networks (GAN)

GAN [8] is a method of a generative network using deep learning. It is divided into two parts:

A. The generator, which is an unsupervised model that takes random data input, usually from Gaussian distribution. It aims to deliver a result that can convince discriminator models that it is real.
B. The discriminator, a supervised model trained with actual data from a dataset and fake data from the generator, has the objective of distinguishing one from the other.

Both models are trained together using a loss function defined by the authors as a two-player minimax game below, where G is the generator and D is the discriminator:

$$min_G max_D V(D, G) = E_{x \sim p_{data}(x)}[\log D(x)] + E_{z \sim p_z}[\log\left(1 - D\left(G(z)\right)\right)] \quad (1)$$

The GAN model is then trained until the generator and discriminator models find an equilibrium. So the discriminator can no longer identify the difference between data generated by the generator and real data.

GAN is a fascinating field of work rapidly evolving and applies to many different problems and experiments [9].

Objective

This work aims to do a systematic review of published and pre-print works that apply GANs to image 2D object detection tasks, alone or in combination with existing object detection methods, and compare their methods and frameworks. The results of this review will evaluate the viability of GAN applied to OD tasks as a potential field of study and applied in future works.

Materials and Methods

We searched many academic and Artificial Intelligence community databases to present a comprehensive overview of GAN applications for 2D Image object detection [10-13].

Since it is a rapidly evolving field, many papers are yet to be published or as pre-prints. Therefore,

the keywords used for the search were: GAN, Object, Detection, Generative, and Adversarial. From the many works found, we first filtered the results by their titles, eliminating all the ones that were not relevant, and then by their abstracts. Since this work focuses on combining GAN techniques with object detection tasks, all papers that deviate from that were discarded, including the many papers that use GANs for data augmentation or 3D object detection.

We selected and analyzed papers with an evaluation of the methods and models used and the results obtained.

Results and Discussion

GAN and Object Detection are very popular themes in the academy. The initial search in Science Direct [11] by the keywords "generative adversarial" and "object detection" presented 851 results. We did a similar process in arXiv. og [13] with 98 initial results, Google Scholar [10] with 17,700 results, and IEEE Xplore [12] with 391 results. The results were then ranked by relevance and manually filtered according to the chosen criteria. In the end, not many works used GANs in combination with Object Detection tasks as required. Therefore, we chose 28 articles, and 14 were considered relevant to this study. We organized the results in Table 1, considering each paper's objective and proposed framework. Table 2 shows the best Mean Average Precision (map) of the models when compared to the surrogate model used in each paper and the dataset used for evaluation.

The studied authors proposed many approaches to address different tasks related to object detection, most of them to enhance the accuracy of traditional object detection frameworks. For overall object detection purposes, Wang and colleagues [14] propose an extensive trained network (teacher) for object detection and then uses a GAN for knowledge distillation from this network to a much simpler one (student) with better results in testing accuracy than the teacher model. The discriminator, in this case, checks whether the results come from the teacher or the student nets and backpropagate to the student network training. The results showed 2.8% better mAP than the surrogate studied. Prakash and Karam [15] show a baseline network trained with real data and competing with a generator net trained with augmented data. Both networks' results are then considered by a discriminator that distinguishes the results between the baseline and generator models. By the end of the adversarial training, the generator

Table 1. Selected papers proposed frameworks.

Method Objective	Paper	Proposed Framework
Overall Object Detection	[14]	SSD + GAN for Knowledge Distillation
	[15]	Competitive Object Detection Networks
Pedestrian Detection	[16]	GAN for synthetic data creation
	[17]	DCGAN + SSD
	[18]	DCGAN + SSD
	[19]	DCGAN + SSD
Small-Object Detection	[20]	Faster R-CNN + GAN
	[21]	GAN + CNN + SSD/Faster R-CNN
	[22]	CNN + ResNet + GAN
Unsupervised Bounding Box Detection	[23]	CNN + GAN + Reinforcement Learning
	[24]	Dilated CNN + GAN with Mask Mean Loss
	[25]	Encoder + Conditional GAN

Table 2. Best mAp(%) of models *vs*. Surrogate Model.

Paper	Best mAp(%) found when compared with Surrogate model and dataset	Surrogate model	Dataset used for evaluation
[14]	2.8	ResNet50	Pascal VOC 2007
[15]	2.56	SSD300	Pascal VOC 2007
[16]	Not Applicable	Not Applicable	Not Applicable
[17]	45.2	SSD	CIFAR-10/100
[18]	39.4	SSD	VOC
[19]	Not Applicable	Not Applicable	Not Applicable
[20]	19.47	Faster R-CNN	Tsinghua-Tencent 100K
[21]	25.1	FRCNN	COWC Dataset
[22]	60	Faster R-CNN (Small Objects)	Tsinghua-Tencent 100K
[23]	Not Applicable	Not Applicable	Not Applicable
[24]	5.37	[23]	Car (Stanford)
[25]	2.6	WCCN VGG16	VOC2007

model can fool the discriminator, and it is then used for inference and testing, presenting 2.56% mAp better than the baseline model. Navidan and colleagues [9] showed that synthetic data creation is a trendy application of GAN. Huang and Hamanan [16] used GAN to generate real-like pedestrian images from synthetic data generated by a game engine. It produces images of pedestrians in unusual scenarios and positions, helping traditional object detection models to improve their ability to detect pedestrians. Dinakaram and colleagues [17-19] used another known and proven ability of Deep Convolutional GAN: an image resolution improvement. All three works combine the GAN's image resolution improvement with SSD to increase its pedestrian detection capabilities in different sizes and distances. This framework can be applied in many scenarios and object classes with significant improvements in the map (Table 2). Small-Object Detection appears as an exponent application for GANs. In Huang and colleagues [20], a GAN is embedded into a Faster R-CNN Network to generate residual representations of small objects to be similar to the ones of big objects, which improves the detection ability of small objects compared to a vanilla Faster R-CNN network. Results show around 19.5% better performance in small object detection than a regular Faster R-CNN. Rabbi and colleagues [21] created a framework that uses a GAN to create high-resolution images from low-resolution images as input. The discriminator compares a real high-resolution image to the generated image. It then uses a different CNN to detect edges and improve the resolution to finally use SSD or a Faster R-CNN to detect the objects, improving the mAP performance by 25.1%. Li and colleagues [22] approach the small object detection task similarly to Huang and colleagues [20] by using region proposals. The authors presented a perceptual GAN architecture where the generator creates super-resolved representations of small objects supervised by the discriminator. The framework also uses a residual network in the generator to carry on the small object representation to be added to the generator's last part and create super-resolved features. The discriminator also has a detection and classification

branch to generate the bounding boxes and infer object class, showing 60% better mAP for small object detection than a Faster R-CNN. One of the most exciting characteristics of GANs is the ability to learn tasks in an unsupervised way. Halici and colleagues [23] and Jang and colleagues [24] use this to identify bounding boxes. Furthermore, Halici and colleagues [23] used it to differentiate images generated by the network from the same images generated in a previous network loop iteratively. So, the discriminator output is used as reinforcement learning input to the model. Jang and colleagues [24] approach the problem differently. The generator creates a black mask while the discriminator compares the generated image to the ground truth. The training stops once the generator can fool the discriminator. Diba and colleagues [25] proposed a novel ranking-discriminator network to verify the object class produced by a conditional GAN network trained with inputs from an original image representation created by an encoder network. The framework uses image-proposed regions also to identify the bounding box in a weakly supervised manner. Unsupervised OD using GANs is still a substantially unexplored field with many challenges. Although Halici and colleagues [23] and Jang and colleagues [24] propose novel approaches to this task, the results obtained are far from a state-of-the-art OD framework and do not explore Multi-Object Detection.

Conclusion

In this work, 14 papers were selected based on specific search criteria of object detection frameworks that utilize GANs in their methods. All the analyzed works proposed different approaches to the problem. Some attack object detection as a generic problem, while others have chosen to do specific tasks such as small objects or pedestrian detectors. Among the proposed frameworks, GAN was used as many tools: image enhancement, data generation, and knowledge distillation. We conclude that GAN's application to the Object Detection task does not have a preferred framework among the academic and Artificial Intelligence communities; besides, all the evaluated papers showed inspiring results. However, it presents a promising field of study to be developed in future works. In this study, we also brought up the relatively unexplored potential of unsupervised OD using GAN. It is specifically exciting if we consider the many GAN frameworks that have been proposed with multiple applications and exciting results.

References

1. Zou Z,et al. Object detection in 20 years: A survey. arXiv preprint arXi 2019;1905.05055.
2. Girshick R, et al. Rich feature hierarchies for accurate object detection and semantic segmentation. In: Proceedings of the IEEE conference on computer vision and pattern recognition. IEEE Conference 2014:580-587.
3. Girshick R. Fast r-cnn. In: Proceedings of the IEEE international conference on computer vision. IEEE Conference 2015:1440-1448.
4. Kaiming HE, et al. Spatial pyramid pooling in deep convolutional networks for visual recognition. IEEE transactions on pattern analysis and machine intelligence IEEE 2015;37(9):1904-1916.
5. Ren S,et al. Faster r-cnn: Towards real-time object detection with region proposal networks. Advances in Neural Information Processing Systems. 2015;28:91-99.
6. Redom J, et al. You only look once: Unified, real-time object detection. In: Proceedings of the IEEE conference on computer vision and pattern recognition. IEEE 2016:779-788.
7. Liu W,et al. Ssd: Single shot multibox detector. In: European conference on computer vision. Springer, Cham. 2016:21-37.
8. Goodfellow I, et al. Generative adversarial nets. ACM Communications 2014:27.
9. Navidan H, et al. Generative Adversarial Networks (GANs) in networking: A comprehensive survey & evaluation. Computer Networks 2021:108-149.
10. Google Scholar. Initial Page. Available at: <https://scholar.google.com/>. Access in: Jul 25th, 2021.
11. Science Direct. Initial Page. Available at: < https://www.sciencedirect.com/>. Access in: Jul 25th, 2021.
12. IEEE Xplore. Initial Page. Available at: <https://ieeexplore.ieee.org/Xplore/home.jsp >. Access in: Jul 25th, 2021.
13 arXiv.og. Initial Page. Available at: < https://arxiv.org/>. Access in: Jul 25th, 2021.
14. Wang W, et al. Gan-knowledge distillation for one-stage object detection. IEEE Access 2020;8:60719-60727.

15. Prakash CD, Karam LJ. It GAN DO better: GAN-based detection of objects on images with varying quality. arXiv preprint arXiv 2019;1912.01707.
16. Huang S, Ramanan D. Expecting the unexpected: Training detectors for unusual pedestrians with adversarial imposters. In: Proceedings of the IEEE Conference on Computer Vision and Pattern Recognition 2017:2243-2252.
17. Dinakaran RK, et al. Deep learning based pedestrian detection at distance in smart cities. In: Proceedings of SAI Intelligent Systems Conference. Springer, Cham, 2019:588-593.
18. Dinakaran R, et al. Distant pedestrian detection in the wild using single shot detector with deep convolutional generative adversarial networks. In: 2019 International Joint Conference on Neural Networks (IJCNN) IEEE 2019:1-7.
19. Dinakaran R, Zhang L, Jiang R. In-vehicle object detection in the wild for driverless vehicles. In: Developments of Artificial Intelligence Technologies in Computation and Robotics: Proceedings of the 14th International FLINS Conference (FLINS 2020) 2020:1139-1147.
20. Huang W, Huang M, Zhang Y. Detection of traffic signs based on combination of GAN and faster-RCNN. In: Journal of Physics: Conference Series. IOP Publishing 2018:012159.
21. Rabbi J, et al. Small-object detection in remote sensing images with end-to-end edge-enhanced GAN and object detector network. Remote Sensing 2020;12(9):1432.
22. Li J, et al. Perceptual generative adversarial networks for small object detection. In: Proceedings of the IEEE conference on computer vision and pattern recognition. IEEE 2017:1222-1230.
23. Halici E, Alatan AA. Object localization without bounding box information using generative adversarial reinforcement learning. In: 2018 25th IEEE International Conference on Image Processing (ICIP). IEEE 2018:3728-3732.
24. Jang H, et al. Generative object detection: Erasing the boundary via adversarial learning with mask. In: 2019 IEEE 2nd International Conference on Information Communication and Signal Processing (ICICSP). IEEE 2019:495-499.
25. Diba A, et al. Weakly supervised object discovery by generative adversarial & ranking networks. In: Proceedings of the IEEE/CVF Conference on Computer Vision and Pattern Recognition Workshops 2019.

Instructions for Authors

The Authors must indicate in a cover letter the address, telephone number and e-mail of the corresponding author. The corresponding author will be asked to make a statement confirming that the content of the manuscript represents the views of the co-authors, that neither the corresponding author nor the co-authors have submitted duplicate or overlapping manuscripts elsewhere, and that the items indicated as personal communications in the text are supported by the referenced person. Also, the protocol letter with the number should be included in the submission article, as well as the name of sponsors (if applicable).

Manuscripts may be submitted within designated categories of communication, including:

- Original basic or clinical investigation (original articles on topics of broad interest in the field of bioengineering and biotechnology applied to health). We particularly welcome papers that discuss epidemiological aspects of international health, clinical reports, clinical trials and reports of laboratory investigations.
- Case presentation and discussion (case reports must be carefully documented and must be of importance because they illustrate or describe unusual features or have important practice implications).
- Brief reports of new methods or observations (short communications brief reports of unusual or preliminary findings).
- State-of-the-art presentations (reviews on protocols of importance to readers in diverse geographic areas. These should be comprehensive and fully referenced).
- Review articles (reviews on topics of importance with a new approach in the discussion). However, review articles only will be accepted after an invitation of the Editors.
- Letters to the editor or editorials concerning previous publications (correspondence relating to papers recently published in the Journal, or containing brief reports of unusual or preliminary findings).
- Editor's corner, containing ideas, hypotheses and comments (papers that advance a hypothesis or represent an opinion relating to a topic of current interest).
- Innovative medical products (description of new biotechnology and innovative products applied to health).
- Health innovation initiatives articles (innovative articles of technological production in Brazil and worldwide, national policies and directives related to technology applied to health in our country and abroad).

The authors should checklist comparing the text with the template of the Journal.

Supplements to the JBTH include articles under a unifying theme, such as those summarizing presentations of symposia or focusing on a specific subject. These will be added to the regular publication of the Journal as appropriate, and will be peer reviewed in the same manner as submitted manuscripts.

Statement of Editorial Policy

The editors of the Journal reserve the right to edit manuscripts for clarity, grammar and style. Authors will have an opportunity to review these changes prior to creation of galley proofs. Changes in content after galley proofs will be sent for reviewing and could be required charges to the author. The JBTH does not accept articles which duplicate or overlap publications elsewhere.

Peer-Review Process

All manuscripts are assigned to an Associate Editor by the Editor-in-Chief and Deputy Editor, and sent to outside experts for peer review. The Associate Editor, aided by the reviewers' comments, makes a recommendation to the Editor-in-Chief regarding the merits of the manuscript. The Editor-in-Chief makes a final decision to accept, reject, or request revision of the manuscript. A request for revision does not guarantee ultimate acceptance of the revised manuscript.

Manuscripts may also be sent out for statistical review ou *ad hoc* reviewers. The average time from submission to first decision is three weeks.

Revisions

Manuscripts that are sent back to authors for revision must be returned to the editorial office by 15 days after the date of the revision request. Unless the decision letter specifically indicates otherwise, it is important not to increase the text length of the manuscript in responding to the comments. The cover letter must include a point-by-point response to the reviewers and Editors comments, and should indicate any additional changes made. Any alteration in authorship, including a change in order of authors, must be agreed upon by all authors, and a statement signed by all authors must be submitted to the editorial office.

Style

Manuscripts may be submitted only in electronic form by www.jbth.com.br. Each manuscript will be assigned a registration number, and the author notified that the manuscript is complete and appropriate to begin the review process. The submission file is in OpenOffice, Microsoft Word, or RTF document file format for texts and JPG (300dpi) for figures.

Authors must indicate in a cover letter the address, telephone number, fax number, and e-mail of the corresponding author. The corresponding author will be asked to make a statement confirming that the content of the manuscript represents the views of the co-authors, that neither the corresponding author nor the co-authors have submitted duplicate or overlapping manuscripts elsewhere, and that the items indicated as personal communications in the text are supported by the referenced person.

Manuscripts are to be typed as indicated in Guide for Authors, as well as text, tables, references, legends. All pages are to be numbered with the order of presentation as follows: title page, abstract, text, acknowledgements, references, tables, figure legends and figures. A running title of not more than 40 characters should be at the top of each page. References should be listed consecutively in the text and recorded as follows in the reference list, and must follow the format of the National Library of Medicine as in Index Medicus and "Uniform Requirements for Manuscripts Submitted to Biomedical Journals" or in "Vancouver Citation Style". Titles of journals not listed in Index Medicus should be spelled out in full.

Manuscript style will follow accepted standards. Please refer to the JBTH for guidance. The final style will be determined by the Editor-in-Chief as reviewed and accepted by the manuscript's corresponding author.

Approval of the Ethics Committee

The JBTH will only accept articles that are approved by the ethics committees of the respective institutions (protocol number and/or approval certification should be sent after the references). The protocol number should be included in the end of the Introduction section of the article.

Publication Ethics

Authors should observe high standards with respect to publication ethics as set out by the International Committee of Medical Journal Editors (ICMJE). Falsification or fabrication of data, plagiarism, including duplicate publication of the authors' own work without proper citation, and misappropriation of the work are all unacceptable practices. Any cases of ethical misconduct are treated very seriously and will be dealt with in accordance with the JBTH guidelines.

Conflicts of Interest

At the point of submission, each author should reveal any financial interests or connections, direct or indirect, or other situations that might raise the question of bias in the work reported or the conclusions, implications, or opinions stated - including pertinent commercial or other sources of funding for the individual author(s) or for the associated department(s) or organizations(s), and personal relationships. There is a potential conflict of interest when anyone involved in the publication process has a financial or other beneficial interest in

the products or concepts mentioned in a submitted manuscript or in competing products that might bias his or her judgment.

Material Disclaimer

The opinions expressed in JBTH are those of the authors and contributors, and do not necessarily reflect those of the SENAI CIMATEC, the editors, the editorial board, or the organization with which the authors are affiliated.

Privacy Statement

The names and email addresses entered in this Journal site will be used exclusively for the stated purposes of this journal and will not be made available for any other purpose or to any other party.

Brief Policies of Style

Manuscript	Original	Review	Birief Comunication	Case Report	Editorial ; Letter to the Editor; Editor' s Corner	Innovative Medical Products	State-of-the-Art	Health Innovation Initiatives
Font Type	Times or Arial	Times or Arial	Times or Arial	Times or Arial	Times or Arial	Times or Arial	Times or Arial	Times or Arial
Number of Words – Title	120	90	95	85	70	60	120	90
Font Size/Space-Title	12; double space	12; double space	12; double space	12; double space	12; double space	12; double space	12; double space	12; double space
Font Size/Space-Abstracts/Key Words and Abbreviations	10; single space	10; single space	10; single space	10; single space	-	-	10; single space	10; single space
Number of Words – Abstracts/Key Words	300/5	300/5	200/5	250/5	-	-	300/5	300/5
Font Size/Space-Text	12; Double space	12; Double space	12; Double space	12; Double space	12; Double space	12; Double space	12; Double space	12; Double space
Number of Words – Text	5,000 including spaces	5,500 including spaces	2,500 including spaces	1,000 including spaces	1,000 including spaces	550 including spaces	5,000 including spaces	5,500 including spaces
Number of Figures	8 (title font size 12, double space)	3 (title font size 12, double space)	2 (title font size 12, double space)	2 (title font size 12, double space)	-	2 (title font size 12, double space)	8 (title font size 12, double space)	8 (title font size 12, double space)
Number of Tables/Graphic	7 title font size 12, double space	2 title font size 12, double space	2(title font size 12, double space)	1(title font size 12, double space)	-	-	7 title font size 12, double space	4 title font size 12, double space
Number of Authors and Co-authors*	15	10	5	10	3	3	15	10
References	20 (font size 10,single space	30(font size 10,single space	15 (font size 10,single space)	10 (font size 10,single space)	10 (font size 10,single space	5(font size 10,single space	20 (font size 10,single space	20

*First and last name with a sequencing overwritten number. Corresponding author(s) should be identified with an asterisk; Type 10, Times or Arial, single space. Running title of not more than 40 characters should be at the top of each page. References should be listed consecutively in the text. References must be cited on (not above) the line of text and in brackets instead of parentheses, e.g., [7,8]. References must be numbered in the order in which they appear in the text. References not cited in the text cannot appear in the reference section. References only or first cited in a table or figures are numbered according to where the table or figure is cited in the text. For instance, if a table is placed after reference 8, a new reference cited in table 1 would be reference 9.1 would be reference 9.

Checklist for Submitted Manuscripts

❑1. Please provide a cover letter with your submission specifying the corresponding author as well as an address, telephone number and e-mail.

❑2. Submit your paper using our website www.jbth.com.br. Use Word Perfect/Word for Windows, each with a complete set of original illustrations.

❑3. The entire manuscript (including tables and references) must be typed according to the guidelines instructions.

❑4. The order of appearance of material in all manuscripts should be as follows: title page, abstract, text, acknowledgements, references, tables, figures/graphics/diagrams with the respective legends.

❑5. The title page must include a title of not more than three printed lines (please check the guidelines of each specific manuscript), authors (no titles or degrees), institutional affiliations, a running headline of not more than 40 letters with spaces.

❑6. Acknowledgements of persons who assisted the authors should be included on the page preceding the references.

❑7. References must begin on a separate page.

❑8. References must be cited on (not above) the line of text and in brackets instead of parentheses, e.g., [7,8].

❑9. References must be numbered in the order in which they appear in the text. References not cited in the text cannot appear in the reference section. References only or first cited in a table or figures are numbered according to where the table or figure is cited in the text. For instance, if a table is placed after reference 8, a new reference cited in table 1 would be reference 9.

❑10. Reference citations must follow the format established by the "Uniform Requirements for Manuscripts Submitted to Biomedical Journals" or in "Vancouver Citation Style".

❑11. If you reference your own unpublished work (i.e., an "in press" article) in the manuscript that you are submitting, you must attach a file of the "in press" article and an acceptance letter from the journal.

❑12. If you cite unpublished data that are not your own, you must provide a letter of permission from the author of that publication.

❑13. Please provide each figure in high quality (minimum 300 dpi: JPG or TIF). Figure must be on a separate file.

❑14. If the study received a financial support, the name of the sponsors must be included in the cover letter and in the text, after the author's affiliations.

❑15. Provide the number of the Ethics Committees (please check the guidelines for authors).